TOPPING OFF THE CAPSTONE: CONSTRAINTS ON THE TIMING OF DEFORMATIONAL FABRIC DEVELOPMENT: CA. 1780 MA BIG SKY OROGENY, SOUTHWESTERN MONTANA

An Undergraduate Research Scholars Thesis

by

BRANDON M. GEDDIE

Submitted to the Undergraduate Research Scholars program
Texas A&M University
in partial fulfillment of the requirements for the designation as an

UNDERGRADUATE RESEARCH SCHOLAR

Approved by
Research Advisor: Dr. Brent V. Miller

May 2016

Major: Geology

TABLE OF CONTENTS

Page

ABSTRACT

Constraints on the Timing of Deformational Fabric Development: Ca. 1780 Ma Big Sky Orogeny, Southwestern Montana

Brandon M. Geddie
Department of Geology and Geophysics
Texas A&M University

Research Advisor: Dr. Brent V. Miller
Department of Geology and Geophysics

The study of ancient collisional belts gives insight into the tectonic settings that shaped the continents today. The Big Sky orogeny, at ca. 1800-1760 million years ago, marks the suturing of two Archean cratons that formed part of ancient North America (Laurentia) during the Proterozoic Eon. The "Topping off the Capstone" initiative at Texas A&M University engages undergraduate students to pursue research using geochronological data to unravel the poorly constrained timing of the metamorphism associated with the Big Sky orogeny throughout the Highland Mountain in southwestern Montana. One persistent problem in this region is the partial resetting of geochronometers due to later hydrothermal events associated with the Cretaceous (~80-70 million years ago) assembly of the Rocky Mountains. In order to try to unravel these complexities to normal applications of U-Pb geochronometers this study evaluated the use of step-wise dissolution of zircons from two granitoid intrusions. Analysis from one sample shows that multiple leach steps are all in agreement and indicate crystallization of the granitoid during the Big Sky orogeny at 1787±56 million years ago with Cretaceous partial resetting. The other sample, which shows significantly more Pb-loss, did not produce Big Sky ages for leach steps. However, the final dissolution analyses of five zircons produced a Big Sky age of 1753±30 million years ago. These ages are in agreement with (presumed) metamorphic

monazite ages of 1765.6±4.3 Ma and 1784±19 Ma, confirming Big Sky age metamorphism and partial melting to produce the granitoid intrusions. These geochronologic data coupled with cathodoluminescence images confirm similar results obtained in the nearby Tobacco Root Mountains. The "step-wise" analysis used here gives a new methodology to more clearly determine ages from zircons that would otherwise provide only ambiguous age results.

DEDICATION

This thesis is dedicated to my parents Dr. Gwynn Geddie and Mrs. Lynn Geddie and my beautiful wife Kari. Your love and support has been the backbone of any success I achieve. As I grow as a scientist I will strive to make you proud and be worthy of all you have given me.

ACKNOWLEDGMENTS

A very special thank you to Dr. Brent V. Miller. His influence and mentorship throughout the year of this project is above and beyond what any student could expect from their undergraduate advisor. He is an inspiration to any aspiring scientist.

Thank you to Mike Deluca and David Lewis for their help and advice.

Thank you to the 2015 Texas A&M University Montana Field Camp for their assistance in gathering samples.

Thank you to Kari Geddie for her masterful help in digital imagery.

Use of the TAMU Materials Characterization Facility and Dr. Andrew Mott are acknowledged.

Thank you to the Texas A&M University L.A.U.N.C.H. Undergraduate Research Scholars program and team members for allowing me to do this project and for the funding provided.

Thank you to Dr. Houser and the College of Geosciences for their help funding of my research.

Thank you to the Terry Foundation for funding my education and always reminding me to not squander the gifts I have been given.

FIGURES AND TABLES

Tables Page

CHAPTER I

INTRODUCTION

1.1 Background

The North American craton was formed from seven Archean provinces, the Wyoming, Slave, Nain, Hearne, Rae, and Burwell. Their stabilization and amalgamation together created the protocraton Laurentia during the Paleoproterozoic Era at about 2500-1600 million years ago (Ma). An extraordinary laboratory for studying the framework of the North American continent is preserved in the Wyoming province, which covers Wyoming and parts of the surrounding states (fig. 1.1). Bounded by three Paleoproterozoic orogenic belts, the Cheyenne belt to the south, the Trans-Hudson orogeny to the east, and the Great Falls Tectonic Zone to the northwest, a history of plate tectonics of over three billion years have been recorded there in the subsurface (Condit et al., 2015; Mueller et al., 2005a). Laramide uplifting brought the cores of fault blocks to the surface exposing Archean and Proterozoic rocks. While these outcrops are scattered and mostly discontinuous, they provide an excellent record of tectonic activity over billions of years.

The ages of rock formation (geochronology) can help to reconstruct ancient plate tectonic events. Analyses of radiogenic isotopes, particularly the decay of Uranium to Lead (U-Pb), gives us quantitative rock age data to work with. The minerals zircon and monazite both allow radioactive Uranium to substitute into their crystal lattices, but not radiogenic lead, and thus they are good geochronometers. This project took advantage of monazite and zircon minerals, fairly ubiquitous accessory minerals, to date the formation of intrusive igneous rocks that have clear field relationships with regional metamorphic and tectonic events. However, previous studies

have determined that these minerals show extreme overprinting and long histories of multiple orogenic events, which complicates the interpretation of age data. Radiation damage causing Pb loss and thermotectonic events causing age resets are believed to lie at the root of these complications.

This study seeks to evaluate what can be done to make the interpretation of U-Pb age data more straightforward and to answer such questions as: What, if any, are the valid ways of interpreting sample ages with severe disruption to the U-Pb systematics? Can fine-tuning current methods bring us a better understanding? These questions are addressed here using step-leach analyses of zircon and monazite crystals from two intrusions in the Highland Mountains of southwestern Montana, an area known to be problematic for geochronology due to highly metamict Zircons.

1.2 The Wyoming Province

The Wyoming Province is ~500,000 km^2 and is subdivided into three subprovinces, the Montana metasedimentary province (MMP), the Beartooth-Bighorn magmatic zone (BBM), and the Southern accreted terranes (SAT) (Mueller and Frost, 2006). The oldest, the MMP, is characterized as a series of supracrustal metamorphic rocks, quartzofeldspathic gneisses, and other granitoids (Condit et al., 2015). The Highland, Tobacco Root, Greenhorn Mountains and the Ruby, Gravelly, Madison, and Southern Madison ranges are all located within the MMP. A distinct characteristic of the province is its carbonate-quartzite-pelite association, though quartzofeldspathic gneisses are much more abundant (Burger, 2004). Ages for some of the quartzofeldspathic gneisses with igneous protoliths are as old as 3.1 to 3.3 Ga (Burger, 2004; Mogk et al., 1992; Mueller et al., 1993). The younger BBM is dominated by tonalite-

trondhjemite-granodiorite intrusives (Burger, 2004; Mogk et al., 1992). The Beartooth Mountains, Bighorn Mountains, Wind River Range, Teton Range, and the Stillwater complex are some of the major features in the BBM. Ages from 2.7-2.9 Ga have been reported throughout this province (Burger, 2004; Mogk et al., 1992). The BBM and the MMP share an enriched $^{207}Pb/^{204}Pb$ isotopic signature by tonalitic and more evolved rocks (Frost et al., 1998; Mueller and Frost, 2006; Mueller et al., 1993; Wooden and Mueller, 1988). The youngest of the subprovinces, the SAT, also referred to as the Wyoming Greenstone province (Burger, 2004), is a product of crustal growth from a series of three discrete pulses along the southern margin of the Wyoming craton at 2.71-2.67, 2.65-2.62, and 2.55-2.50 Ga (Chamberlain et al., 2003; Mueller and Frost, 2006). The Medicine Bow and Sierra Madre Mountains as well as the Laramie Range are located here.

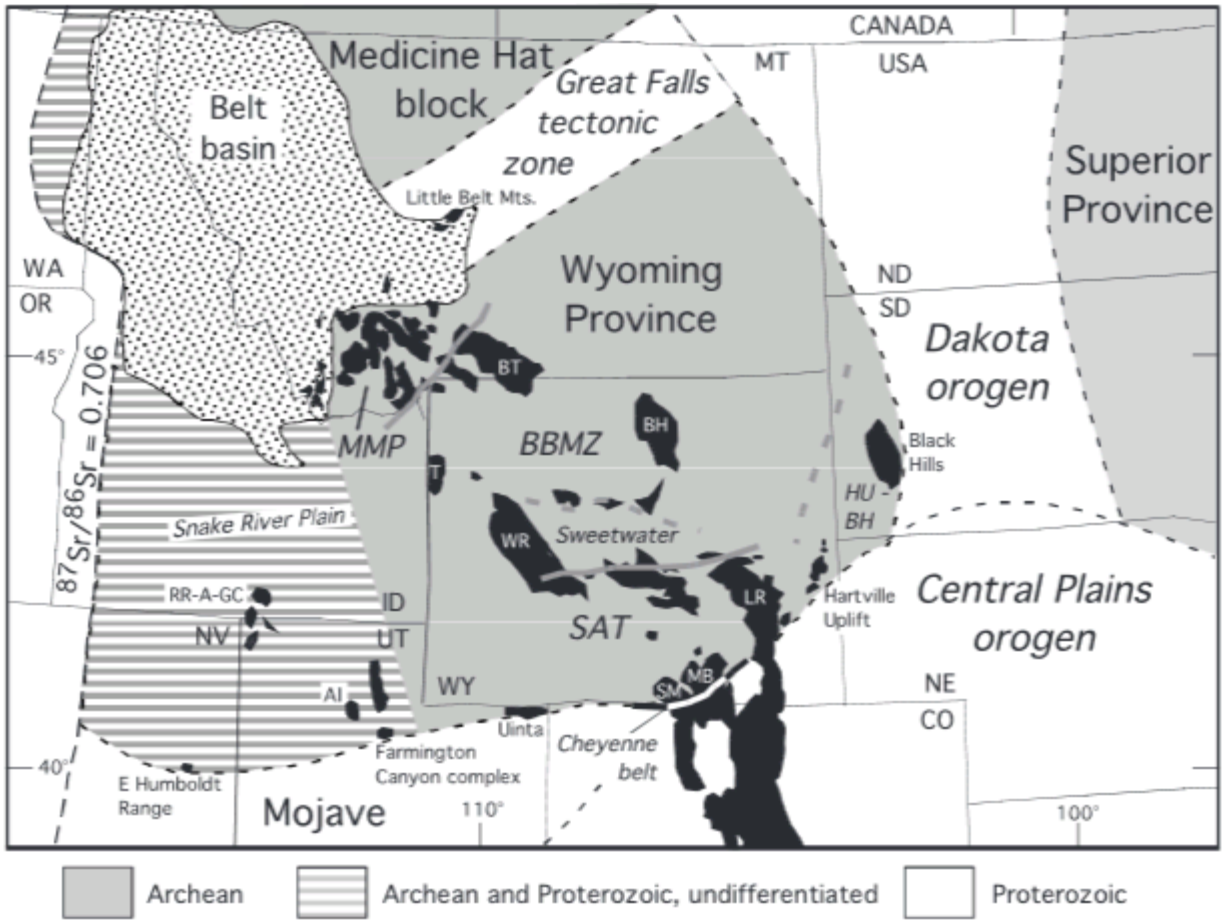

Figure 1.1. Archean cratonic provinces of Southwestern Laurentia. Arrows indicate the general convergence directions of Paleoproterozoic orogenic belts adapted from (Mueller and Frost, 2006).

1.3 The Highland Mountains

The Highland Mountains (HM) gneiss complex has been classified as a fault-bounded structural dome that holds the westernmost Archean/Proterozoic rocks in the Wyoming Province that covers ~400 km^2 (O'Neill et al., 1988). A high-grade, migmatitic, metamorphosed quartzofeldspathic core overlain by metamorphosed supracrustal rocks dominates the HM (O'Neill et al., 1988). Metamorphic conditions in the Highland Mountains during the Precambrian reached temperatures of >750 ^{o}C and pressures >8.6 kbars (Mueller et al., 2005b; O'Neill et al., 1988). Major faulting in the north and east of the HM are younger than the gneiss

domes structure and bring the Precambrian rocks into juxtaposition with younger Phanerozoic rocks (O'Neill et al., 1988). The metamorphic rocks in the area generally consist of a massive leucocratic gneiss (mapped X(A)q) in O'Neill (1996), and a well-foliated quartz-feldspar-biotite gneiss mapped (X(A)qf) (see fig. 1.3). Sills and dikes of aplite and pegmatite are found throughout the gneiss complex and range from quartz monzonite to granite (O'Neill et al., 1988). These igneous intrusions are thought to have been produced from anatectic melts during peak metamorphism in the Paleoproterozoic.

1.4 The Big Sky Orogeny

The Big Sky orogeny (1780-1760 Ma; Harms et al., 2008) is a late Paleoproterozoic thermotectonic event that deformed much of the northern margin of the Wyoming Province (Condit et al, 2015). The age of Big Sky becomes younger further from the orogen core in a southeast direction (Fig. 1.2) from ca. 1810-1780 Ma in the Highland Mountains, to ca. 1780-1720 Ma in the Ruby Range, Tobacco Root Mountains, and northwestern most Northern Madison Range, and 1750-1720 Ma in central Northern Madison Range (Condit et al. 2015). Regional geology suggests this happened during an accreted arc terrain collision and the amalgamation of Medicine Block and Wyoming provinces, leaving a SW-NE trending zone of deformation in the Great Falls Tectonic Zone (GFTZ in Fig. 1.2; Harms et al., 2006). An extreme reworking of preexisting rocks occurred with pressures and temperatures characteristic of the deep roots or crystalline cores of collisional orogens (Harms et al., 2006). Peak metamorphic conditions are preserved with pressures >1.0 GPa and temperatures >700℃ in a clockwise pressure-temperature loop typical of tectonic burial beneath collisional orogens (Condit et al., 2015; Harms et al., 2006).

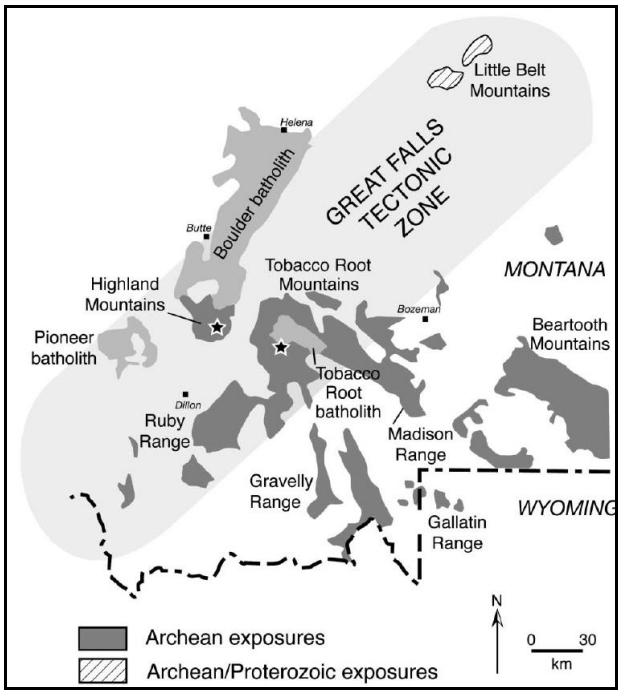

Figure 1.2. Generalized locations of Archean basement rock exposures in the Northern Wyoming province (from Mueller et al., 2005).

During the Big Sky orogeny, Precambrian rocks in Southwest Montana became reworked and metamorphosed to granulite and upper-amphibolite facies, with their dominant structure across the region striking NE-SW by foliation and fold axial surfaces (Condit et al, 2015). Outcrop-scale folds, with wavelength and amplitude ranging from centimeters to meters, are common throughout this region (Harms et al., 2004). Peak temperatures caused metasediments to induce anataxis.

1.5 Topping off the Capstone Initiative

Topping off the Capstone is an initiative at Texas A&M University that encourages students who have completed Geol 300 Summer Field Camp to do independent research projects on the rocks found in the Montana Field Camp mapping areas.

Previous mapping projects at Texas A&M, in the Highland Mountains, have demonstrated that tabular granitic intrusions (dikes) both cross-cut and are deformed within the regional deformational fabrics of Archean gneisses that form the crystalline core of the Highland Mountains. Recent studies have demonstrated that the granitic dikes appear to be of two distinct field and petrographic associations, but their age difference has proven difficult to resolve.

A presumed earlier generation of medium-grained, internally deformed and recrystallized, biotite-rich, garnet-bearing granitoid dikes that cut across the gneissic fabric, are locally folded into the gneiss, pinch and swell, and show similar fabrics as the adjacent gneisses. Where less-deformed, these dikes form conduits that focus melt migration from surrounding migmatitic gneiss. Many silver and gold exploration pits are found within or near these dikes, but none were developed into full mining operations. In contrast, a presumed later generation of well preserved, course-grained, graphic igneous texture, granitoid dikes that show no penetrative deformational fabrics and cut more sharply across the gneissic fabric of the country rocks. This generation, while sampled by numerous assay pits, has no associated mining activity. New data is presented in this thesis from petrology and U-Pb geochronology in the Highland Mountains to better distinguish these separate generations of intrusions and answer questions about Big Sky's regional extent and thermal impact throughout southwestern Montana.

1.6 Sample Descriptions and Locations

Sample FC15-005 is a medium grained, biotite-rich garnet-bearing granite (see fig. 1.4). It is located ~15 km to the northwest of Twin Bridges, MT. Access to the outcrop can be gained via a BLM (Bureau of Land Management) road off of the Melrose-Twin Bridges Road. The sample was collected from a granitoid dike with a N-NE trend that varies in width but is approximately 3m wide where it abruptly terminates in a narrow dry creek bed. On the other side of the creek are several inactive silver mines. Many field camp student maps infer a fault, buried by the Quaternary sediments of the creek bed, based on subtle changes in lithologies and orientations of metamorphic foliation. A fault here could also explain the focus of this small creek bed for silver mines and exploration pits. O'Neill (1996) mapped the area as *XS - Igneous and metamorphic rocks, undivided (Early Proterozoic) -- Dense swarm of leucocratic quartz-feldspar sills intruded into crystalline metamorphic rocks* (fig. 1.3).

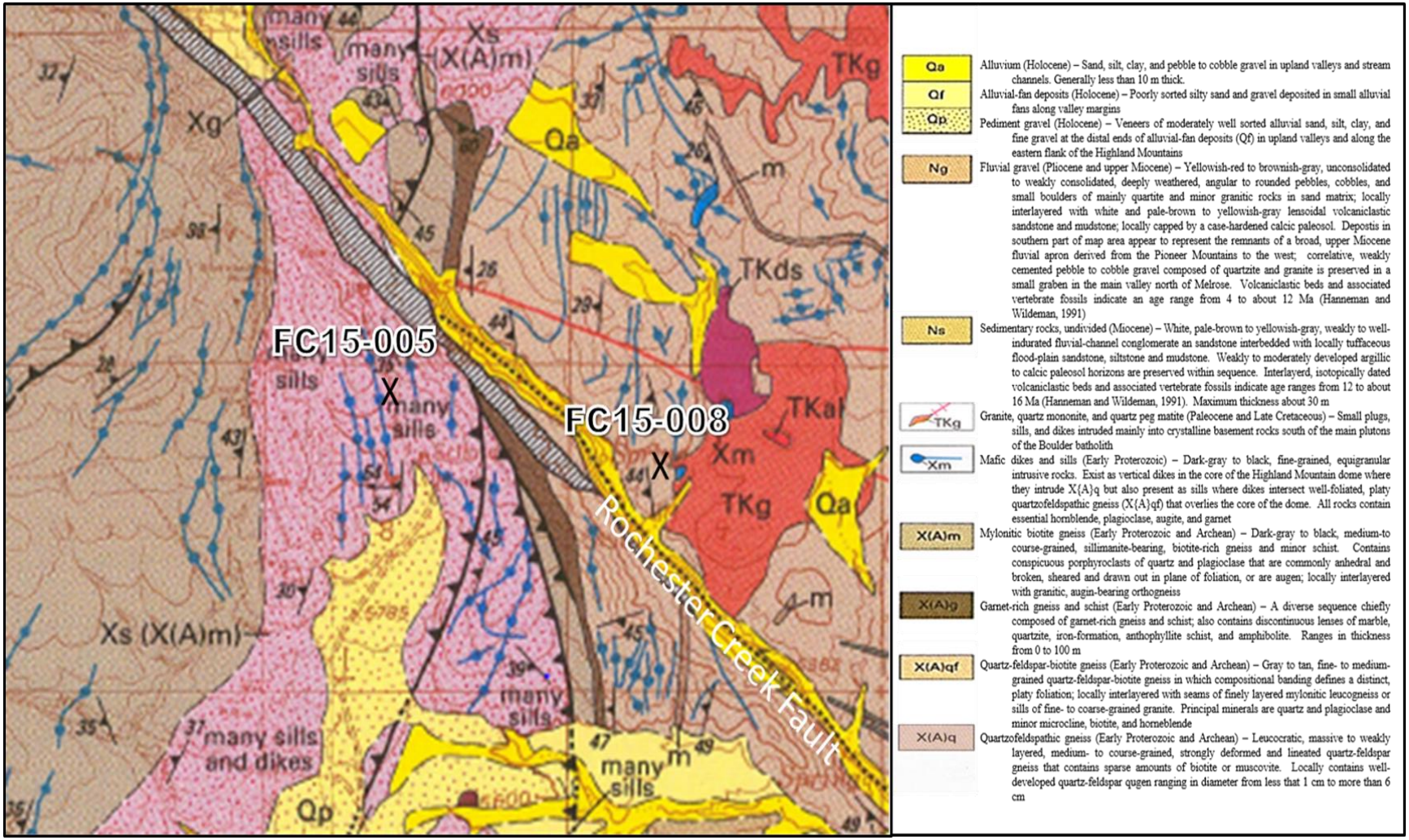

Figure 1.3. Geologic map of the southern Highland Mountains modified from (O'Neill, 1996).

Figure 1.4. Image of sample FC15-005. A medium grained granatoid intrusion showing deformational fabrics throughout. Coin used for scale.

Figure 1.5. Image of outcrop location for FC15-005 modified from Google Earth.

Sample FC15-008 is a coarse grained, leucocratic granite (see fig. 1.6). It is located ~12 km northwest of Twin Bridges, MT. Access can be gained by heading north-east on a private road just off of Melrose-Twin Bridges county road (see fig. 1.7). Rochester creek crosses under both the private and county roads near the turnoff. Around 30 meters to the east a Cretaceous age pluton outcrops marked as Toga in (O'Neill, 1996) which is described as *granite, quartz monzonite, and quartz pegmatite* – "small plugs, sills, and dikes intruded mainly into crystalline basement rocks south of the main plutons of the Boulder batholith" (fig. 1.3). The South Rochester fault is located just to the south under the Melrose-Twin Bridges county road and covered by Quaternary alluvium.

Figure 1.6. Image of FC15-008. Coarse grains with no visible signs of deformation after crystallization. Coin used for scale.

Figure 1.7. Modified image from Google Earth. FC15-008 can be seen as the white outcrop trending northwest-southeast just under the marked yellow pin.

CHAPTER II

METHODS

Samples FC15-005 and FC15-008 were collected during the 2015 Texas A&M Montana Summer Field Camp and prepared at the university's rock crushing and mineral separation labs. Six and five monazite grains were selected from FC15-005 and FC15-008 respectively. Nine zircon grains were selected from each sample. Both monazite and zircon were selected to best represent the range of shape, size, damage, and transparency within the grains of each sample. The zircons in both samples range from euhedral to anhedral, and vary in size (Fig. C1-C2). Sample FC15-005 yielded both clear and metamict grains while FC15-008 lacked clear grains, with instead nearly all brown and highly metamict. The monazites in FC15-005 were about the same size and range from anhedral to subhedral, while those from FC15-008 have significant range in size and are also anhedral to subhedral (Fig. C3-C4). Grains were subjected to combined annealing and multi-step partial dissolution analyses modeled after (Mattinson, 2005) Chemical Abrasion Thermal Ionization Mass Spectrometry (CA-TIMS), but in this study the leachate from each step was collected and analyzed.

This project highlights the chemical analysis in four steps: Step 1) A hotplate leach in a $HF+HNO_3$ acid. Step 2) Strong HF chemical abrasion in a pressurize capsule. Step 3) A hotplate HCl wash. Step 4) Final dissolution of zircon grains in strong HF acid in a pressurized capsule. A more detailed review of laboratory methods can be found in Appendix A.

Uranium and Pb separated from zircon and monazite grains were analyzed using a Thermo-Fisher Triton thermal ionization mass spectrometer housed in the R. Ken Williams ’45 Radiogenic Isotope Geosciences laboratory at Texas A&M University. Data reduction was conducted using Tripoli (Bowring et al., 2011) and YourLab (Schmitz and Schoene, 2007) and data plotted using Isoplot software (Ludwig, 2003).

Another aliquot of zircon and monazite grains were mounted on a 1-inch diameter epoxy puck for cathodoluminescence and backscattered electron imagining using the Cameca SXFive electron microprobe in the Texas A&M University Materials Characterization Facility. Inclusions were also analyzed in the electron microprobe using Energy Dispersive Spectroscopy.

CHAPTER III

RESULTS

3.1 TIMS Analyses

TIMS analyses of all zircons showed a linear trend of the HF + HNO_3 leach (step 1), the chemical abrasion leach (step 2), and the final dissolved zircon solution (step 4) with each grain (see fig. B1-B2 and B6 of Appendix B). Error ellipses representing the HCl wash leach showed a pattern of being large and reversely discordant. By excluding the HCl wash in calculating dates, two zircon age groups were identified in sample FC15-005. Three of the grains showed a Big Sky dates ~1760 Ma. Three other grains showed dates at or near 2300 Ma. One grain plotted at ~1870 Ma but is lumped into the younger group. The zircons that showed similar dates were combined and new dates were recalculated. The initial HF + HNO_3 analyses had a lower (close to 1 or less) radiogenic to common Pb ratio (See Table 1) and was therefore not included in the recalculation. An upper-intercept age of 1787±56 Ma and lower-intercept age of 83±140 Ma were constrained from the younger group of zircons (fig. B3). The other group produced an upper-intercept age of 2297±170 and lower-intercept age of 330±580 Ma (fig. B4). A third round of calculations were done by excluding the chemical abrasion analyses and only plotting the dissolved zircon solution analyses to compare uncertainties between conventional methods and step-wise analysis. Both groups of zircons showed ambiguous ages when plotted unanchored. Only by anchoring a present day lower-intercept was a Big Sky upper-intercept constrained, but with large uncertainties. The older group of zircons failed to produce a reliable date when plotting just the dissolved zircon analyses even with an anchored lower-intercept. Monazites from FC15-005 (fig. C3) plot with little discordance at 1765.5±4.3 Ma (fig. B5).

Zircons from FC15-008 (fig. C2) showed the same initial patterns when plotting all four steps on concordia diagrams. The HCl wash analyses were excluded when calculating single zircon dates and similar patterns of steps 1, 2, and 4 plotting linearly was observed; however, ambiguous upper-intercept dates from ~1400 up to ~2400 did not allow for any correlation between zircons. The chemical abrasion and final dissolved zircon solution analyses were plotted but failed to reduce the uncertainty and discordance. Excluding steps 1, 2, and 3 analyses constrained an age of 1753±30 and 84.4±5.3 Ma (fig. B). Monazites from FC15-008 (fig. C4) produced a Big Sky age of 1784±19 Ma (fig. B9).

3.2 Cathodoluminescence and Microprobe Analyses.

Analyses of zircons under cathodoluminescence (CL) imaging show zoning patterns consistent throughout each grain from FC15-005 (see fig. C5-C6). Apatite inclusions seen in CL and Backscatter images were analyzed using Energy Dispersive Spectroscopy (EDS) (See fig. C5). Zircons from FC15-008 did not show any intact zoning patterns or internal structure that could be confidently identified imaged under CL (see fig. C7-C8). Inclusions found in these grains were analyzed using EDS and identified as xenotime (fig. C9).

CHAPTER IV

CONCLUSION

Data from FC15-005 indicates that analyzing the chemical abrasion solution along with the final dissolved zircon solution provides a wider spread of discordance that fits tightly on a line. This extra step in the methodology will provide lower uncertainty when applied to complex zircons with a deep history of overprinting and Pb-loss. In the zircons from the Highland Mountains, two generations of zircons were identified (see table 1 below), the younger having constrained upper and lower-intercepts of 1787±56 and 83±140 Ma, respectively. The upper intercept is consistent with the age of Big Sky orogeny ca. 1780-1760 (Harms et al., 2004) and the lower intercept is likely from partial resetting during the Cretaceous where faulting and uplifting have been recorded and observed in mining pits (O'Neill and Schmidt, 1989) as seen in the near this sample (fig. 1.5). The older generation of zircons (table 1) produced dates of 2297±170 and 330±580 Ma at the upper and lower-intercepts respectively (fig. B4) which is interpreted as cryptic evidence of the Tendoy/Beaverhead orogeny that has been associated with a rifting event ~2400 Ma in surrounding mountain ranges (Cheney et al., 2004). EDS analysis of inclusions show that apatite is trapped within some of the zircon cores and may lead to fractionation during U-Pb analysis. Future projects would benefit from identifying these grains and excluding them from any geochronological studies to minimize uncertainty in the data.

Constraints on the age of FC15-008 proved far more difficult and use of analyses from steps 1, 2, and 3 were not beneficial (Table 2). Dates were unreliable and did not show any correlation between zircons when using single zircon analysis. Only by taking advantage of traditional

Table 1. Overview of U-Pb data from FC15-005

Sample	**Step 1**	**Step 2**	**Step 3**	**Step 4**	**Date** (single grain analyses)
FC15-005 Zircon 1	Poor correlation coefficient, low radiogenic to common Pb ratio	Good correlation coefficient, high radiogenic to common Pb ratio	Large error ellipse, fractionation, Good correlation coefficient	Good correlation coefficient, high radiogenic to common ratio	Big Sky age (~1760-1780)
FC15-005 Zircon 2	Poor correlation coefficient, low radiogenic to common Pb ratio	Good correlation coefficient, high radiogenic to common Pb ratio	Large error ellipse, fractionation, good correlation coefficient	Good correlation coefficient, high radiogenic to common ratio	~1870 Ma Lumped in with Big Sky zircons
FC15-005 Zircon 3	Poor correlation coefficient, low radiogenic to common Pb ratio	Good correlation coefficient, high radiogenic to common Pb ratio.	Large error ellipse, fractionation, poor correlation coefficient	Good correlation coefficient, high radiogenic to common ratio	~2300 Ma
FC15-005 Zircon 4	Poor correlation coefficient, low radiogenic to common Pb ratio	Good correlation coefficient, high radiogenic to common Pb ratio.	Large error ellipse, fractionation, good correlation coefficient	Good correlation coefficient, high radiogenic to common ratio	~2300 Ma

Table 1 cont.

Sample	**Step 1**	**Step 2**	**Step 3**	**Step 4**	**Date** (single grain analyses)
FC15-005 Zircon 5	Poor correlation coefficient, low radiogenic to common Pb ratio	Good correlation coefficient, high radiogenic to common Pb ratio	Large error ellipse, fractionation, poor correlation coefficient	Good correlation coefficient, high radiogenic to common ratio	Big Sky age (~1760-1780)
FC15-005 Zircon 7	Poor correlation coefficient, low radiogenic to common Pb ratio	Good correlation coefficient, high radiogenic to common Pb ratio	Large error ellipse, fractionation, good correlation coefficient	Good correlation coefficient, high radiogenic to common ratio	Big Sky age (~1760-1780)
FC15-005 Zircon 9	Poor correlation coefficient, low radiogenic to common Pb ratio	Good correlation coefficient, high radiogenic to common Pb ratio.	Large error ellipse, fractionation, good correlation coefficient	Good correlation coefficient, high radiogenic to common ratio	Big Sky age (~1760-1780)

methods (Mattinson, 2005) with the final dissolved zircon analyses were a geologically sensible upper-intercept of 1753±30 Ma and a lower intercept of 84.4±5.3 Ma constrained. Both intercepts are consistent with Big Sky ages and Cretaceous resetting. Inclusions found within zircons from FC15-008 do not indicate a direct link to fractionation and require further study to see what, if any, role the xenotime mineral plays in the evolution of the zircon grains.

Table 2. Overview of U-Pb data from FC15-008**.**

Sample	**Step 1**	**Step 2**	**Step 3**	**Step 4**	**Date**
FC15-008 Zircon 1	Poor correlation coefficient, low radiogenic to common Pb ratio	Poor correlation coefficient, high radiogenic to common Pb ratio	Large error ellipse, fractionation, Good correlation coefficient	Good correlation coefficient, high radiogenic to common ratio	No reliable date found
FC15-005 Zircon 2	Poor correlation coefficient, low radiogenic to common Pb ratio	Poor correlation coefficient, high radiogenic to common Pb ratio	Large error ellipse, fractionation, Good correlation coefficient	Good correlation coefficient, high radiogenic to common ratio	No reliable date found
FC15-005 Zircon 3	Poor correlation coefficient, low radiogenic to common Pb ratio	Poor correlation coefficient, high radiogenic to common Pb ratio	Large error ellipse, fractionation, good correlation coefficient	Good correlation coefficient, high radiogenic to common ratio	No reliable date found
FC15-005 Zircon 5	Poor correlation coefficient, low radiogenic to common Pb ratio	Good correlation coefficient, high radiogenic to common Pb ratio.	Large error ellipse, fractionation, poor correlation coefficient	Good correlation coefficient, high radiogenic to common ratio	No reliable date found
FC15-005 Zircon 9	Poor correlation coefficient, low radiogenic to common Pb ratio	Good correlation coefficient, high radiogenic to common Pb ratio.	Large error ellipse, fractionation, good correlation coefficient	Good correlation coefficient, high radiogenic to common ratio	Big Sky age (~1760-1780)

Key observations were made during this project that will be beneficial to future U-Pb analyses of complex zircons that are highly metamict and produce discordant dates. Using step-wise analysis of zircons that show consistent zoning and internal structure under cathodoluminescence (fig.

C6) will provide an anchoring point for the lower-intercept on a concordia diagram. The spread that is observed on the 206/207 Pb line shows that a tightly fit line can pass through most if not all data points recorded. Zircons from FC15-008 showed more complex U-Pb systematics and better age resolution would require further work, perhaps with more and more-intensive leaching steps. The best defense for this is in the CL images (fig. C7-C8). No internal structure or zoning can be confidently identified and every zircon appears too metamict to prevent fractionation of step analyses. Though an age can be constrained for FC15-008, its data does not abate discordance.

The Big Sky orogeny's impact in the Highland Mountains has been widely documented and the conclusion of this project is continued evidence that the intrusions found in the southern Highland Mountains were greatly influenced by metamorphism ca 1780-1760 Ma. With over a billion years of overprinting and tectonic reworking, U-Pb dating will continue to be a complex and problematic endeavor. Future studies can now take an initial qualitative approach when selecting samples to use step-wise analyses and minimize confusion when trying to calibrate deep time among highly metamict zircons by assessing the internal structure of zircon grains in the initial stages.

REFERENCES

Bowring, J. F., McLean, N. M., and Bowring, S. A., 2011, Engineering cyber infrastructure for U-Pb geochronology: Tripoli and U-Pb_Redux: Geochemistry, Geophysics, Geosystems, v. 12, no. 6, p. n/a-n/a.

Burger, H. R., 2004, General geology and tectonic setting of the Tobacco Root Mountains: Geological Society of America Special Papers, v. 377, p. 1-14.

Chamberlain, K. R., Frost, C. D., and Frost, B. R., 2003, Early Archean to Mesoproterozoic evolution of the Wyoming Province: Archean origins to modern lithospheric architecture: Canadian Journal of Earth Sciences, v. 40, no. 10, p. 1357-1374.

Cheney, J. T., Webb, A. A. G., Coath, C. D., and McKeegan, K. D., 2004, In situ ion microprobe 207Pb/206Pb dating of monazite from Precambrian metamorphic suites, Tobacco Root Mountains, Montana: Geological Society of America Special Papers, v. 377, p. 151-179.

Condit, C. B., Mahan, K. H., Ault, A. K., and Flowers, R. M., 2015, Foreland-directed propagation of high-grade tectonism in the deep roots of a Paleoproterozoic collisional orogen, SW Montana, USA: Lithosphere.

Frost, C. D., Frost, B. R., Chamberlain, K. R., and Hulsebosch, T. P., 1998, The Late Archean history of the Wyoming province as recorded by granitic magmatism in the Wind River Range, Wyoming: Precambrian Research, v. 89, no. 3–4, p. 145-173.

Harms, T. A., Brady, J. B., Burger, H. R., and Cheney, J. T., 2004, Advances in the geology of the Tobacco Root Mountains, Montana, and their implications for the history of the northern Wyoming Province: Geological Society of America Special Papers, v. 377, p. 227-243.

Ludwig, K., 2003. Isoplot 3.00. Berkeley Geochronology Center Special Publication, 4. 70 pp.

Mattinson, J. M., 1994, A Study of Complex Discordance in Zircons Using Step-Wise Dissolution Techniques: Contributions to Mineralogy and Petrology, v. 116, no. 1-2, p. 117-129.

Mattinson, J. M., 2005, Zircon U–Pb chemical abrasion ("CA-TIMS") method: Combined annealing and multi-step partial dissolution analysis for improved precision and accuracy of zircon ages: Chemical Geology, v. 220, no. 1–2, p. 47-66.

Mogk, D. W., Mueller, P. A., and Wooden, J. L., 1992, The nature of Archean terrane boundaries: an example from the northern Wyoming Province: Precambrian Research, v. 55, no. 1-4, p. 155-168.

Mueller, Paul A., Burger, H. R., Wooden, Joseph L., Brady, John B., Cheney, John T., Harms, Tekla A., Heatherington, Ann L., and Mogk, David W., 2005a, Paleoproterozoic Metamorphism in the Northern Wyoming Province: Implications for the Assembly of Laurentia: The Journal of Geology, v. 113, no. 2, p. 169-179.

Mueller, P. A., Burger, H. R., Wooden, J. L., Brady, J. B., Cheney, J. T., Harms, T. A., Heatherington, A. L., and Mogk, D. W., 2005b, Paleoproterozoic Metamorphism in the Northern Wyoming Province: Implications for the Assembly of Laurentia: Journal of Geology, v. 113, no. 2, p. 169-179.

Mueller, P. A., and Frost, C. D., 2006, The Wyoming Province: a distinctive Archean craton in Laurentian North America: Canadian Journal of Earth Sciences, v. 43, no. 10, p. 1391-1397.

Mueller, P. A., Shuster, R. D., Wooden, J. L., Erslev, E. A., and Bowes, D. R., 1993, Age and Composition of Archean Crystalline Rocks from the Southern Madison Range, Montana - Implications for Crustal Evolution in the Wyoming Craton: Geological Society of America Bulletin, v. 105, no. 4, p. 437-446.

O'Neill, J. M., 1996, Geologic map and cross sections of the central and southern Highland Mountains, southwestern Montana, [Reston, Va.] : The Survey ;, 1996., Miscellaneous investigations series: map I-2525.

O'Neill, J. M., and Schmidt, C. J., 1989, Tectonic setting and structural control of gold deposits in cratonic rocks of the Rochester and Silver Star mining districts, Highland Mountains, southwestern Montana.

O'Neill, J. M., Duncan, M. S., and Zartman, R. E., 1988, An early Proterozoic gneiss dome in the Highland Mountains, southwestern Montana: Precambrian and Mesozoic plate margins. Edited by SE, Lewis and RB Berg. Montana Bureau of Mines and Geology, Special Publication, v. 96, p. 81-88.

Schmitz, M. D., and Schoene, B., 2007, Derivation of isotope ratios, errors, and error correlations for U-Pb geochronology using 205Pb-235U-(233U)-spiked isotope dilution thermal ionization mass spectrometric data: Geochemistry, Geophysics, Geosystems, v. 8, no. 8, p. n/a-n/a.

Wooden, J. L., and Mueller, P. A., 1988, Pb, Sr, and Nd isotopic compositions of a suite of Late Archean, igneous rocks, eastern Beartooth Mountains: implications for crust-mantle evolution: Earth and Planetary Science Letters, v. 87, no. 1, p. 59-72.

APPENDIX A

METHODOLOGY EXTENDED

Rock and disc crushers were used to reduce sediment size and desegregate the grains. Use of the Wilfley table removed any light minerals and the remaining grains were run through Methylene Iodide heavy liquids to isolate the heaviest minerals.

Zircon samples were placed in a 7 ml beaker with 500 µl HF, 30 µl HNO_3, and 10.5 M HCl. Beakers were left on a hotplate for four days and then the grains were separated from the leaching acid. This first acid step had not been analyzed in previous projects at Texas A&M but was loaded and ran through Isotopic Dilution Thermal Ionization Mass Spectrometry (ID-TIMS). The grains were placed in Teflon containers for annealing and abrasion in HF and HNO_3 at 900^{o}C for ~10 hours to repair damage due to radiation and strip away damaged outer grain growth. The solution was analyzed through ID-TIMS. The grains were put in 10.5 M HCl and left for ~3 days to leach out any internal damage and Pb loss from the grains. This acid has been discarded in previous projects but was analyzed through ID-TIMS here. The remaining grains were dissolved in HF on a hotplate after ~2 days. These dissolved Zircons were analyzed through ID-TIMS. All chemistry done for ID-TIMS was modeled from the techniques described in (Mattinson, 1994) and (Mattinson, 2005)

Monazite samples were left on a hot plate in 50 µl of HNO_3 and 100 µl of HF overnight to allow the grains to dissolve. The resulting solution was put through the same chemistry used for the Zircons and analyzed with the ID-TIMS.

APPENDIX B

DATA ANALYSIS

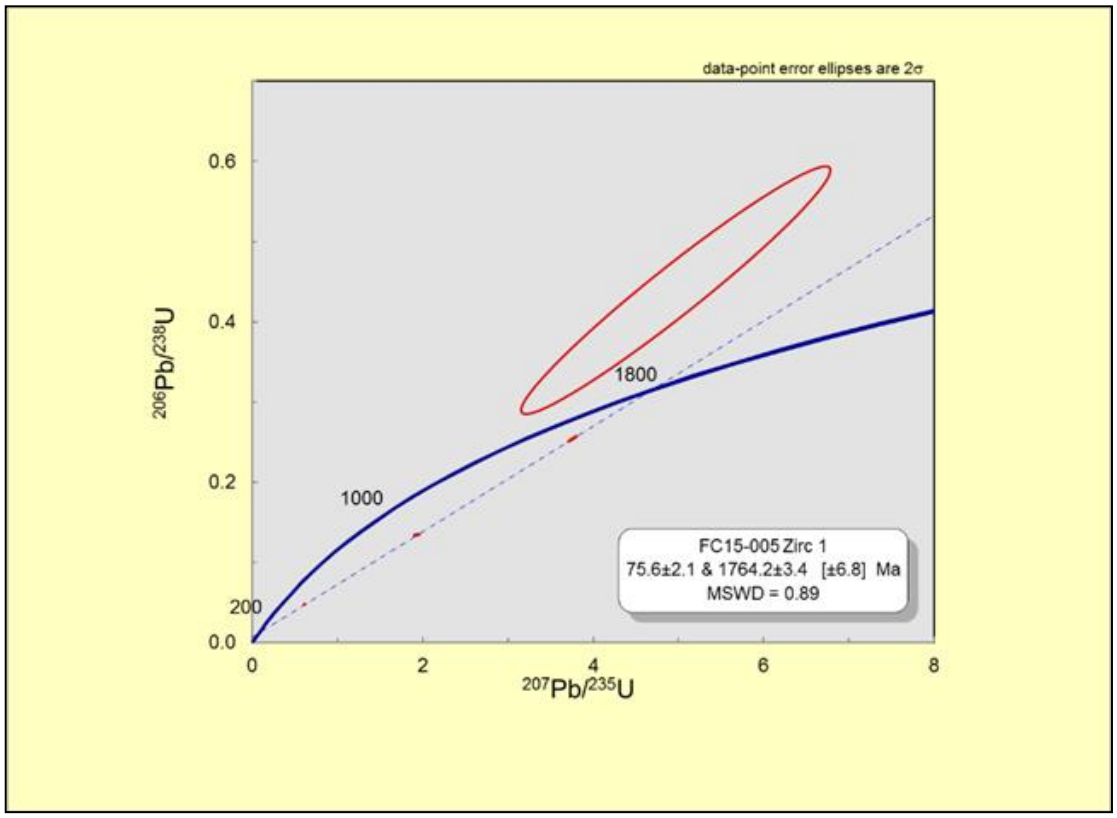

Figure B1. Concordia diagram for FC15-005 Zircon 1. The large ellipse represents the HCl wash analysis. The upper and lower intercept dates of 1764.2±3.4 and 75.6±2.1 Ma do not include the HCl wash data.

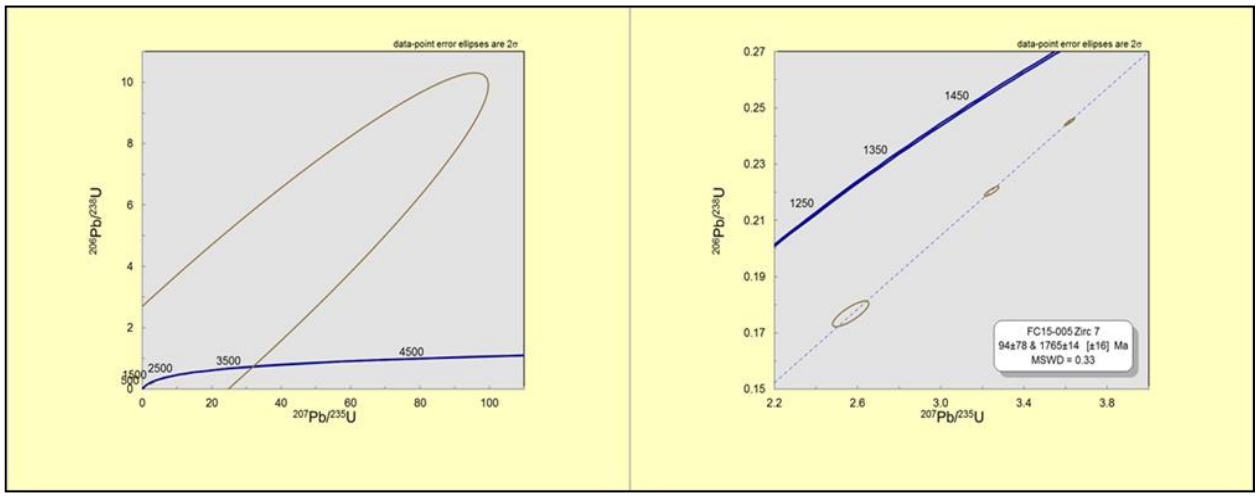

Figure B2. Concordia diagrams for FC15-005 zircon 6. The large error ellipse show on the left diagram represents the HCl wash. The dates of 1765±14 and 94±78 Ma, shown on right, exclude the HCl wash analysis.

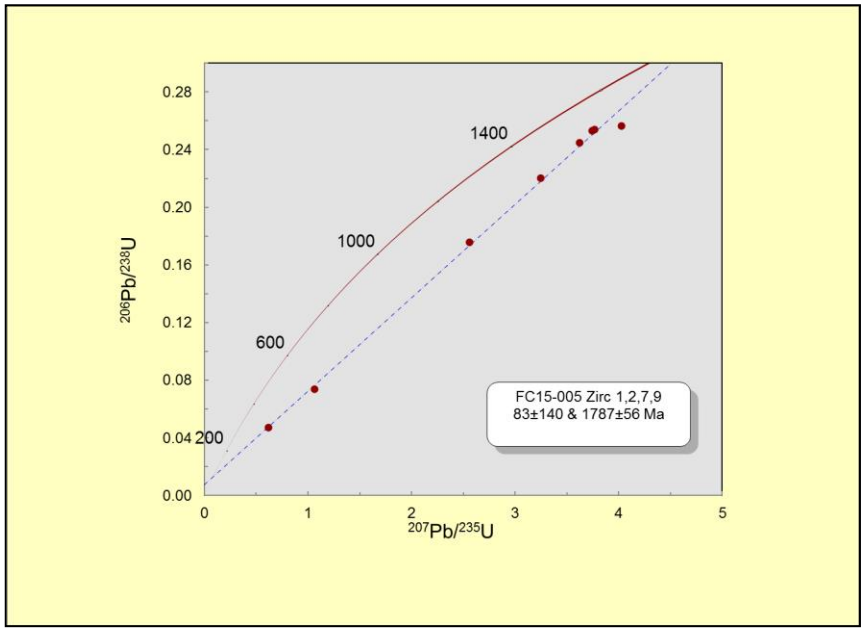

Figure B3. Concordia diagram for FC15-005 zircons 1, 2, 7, and 9. The chemical abrasion (step 2) and final dissolved zircons (Step 4) were plotted together to constrain dates of 1787±56 and 83±140 Ma.

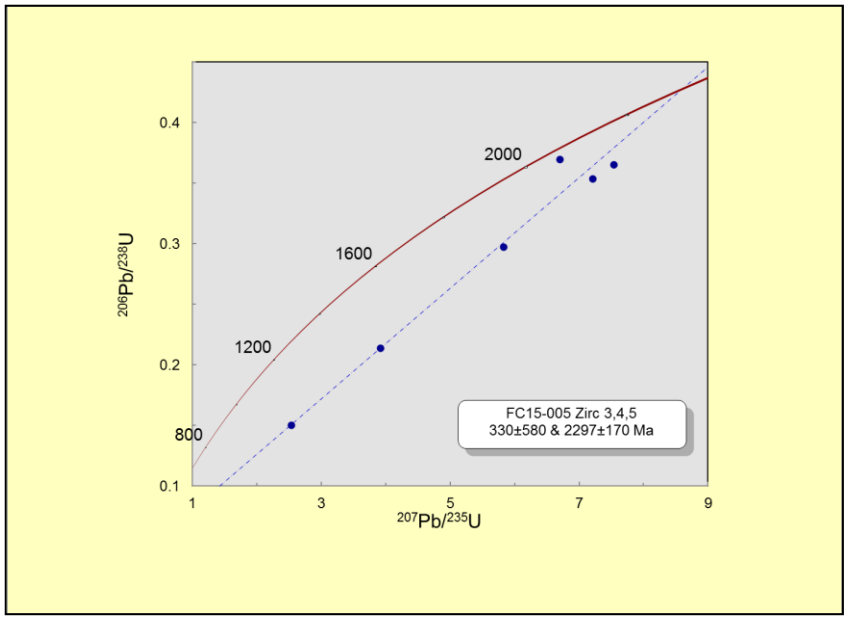

Figure B4. Concordia diagram for FC15-005 zircons 3, 4, and 5. The chemical abrasion (step 2) and final dissolved zircons (Step 4) were plotted together to constrain dates of 2297±170 and 330±580 Ma.

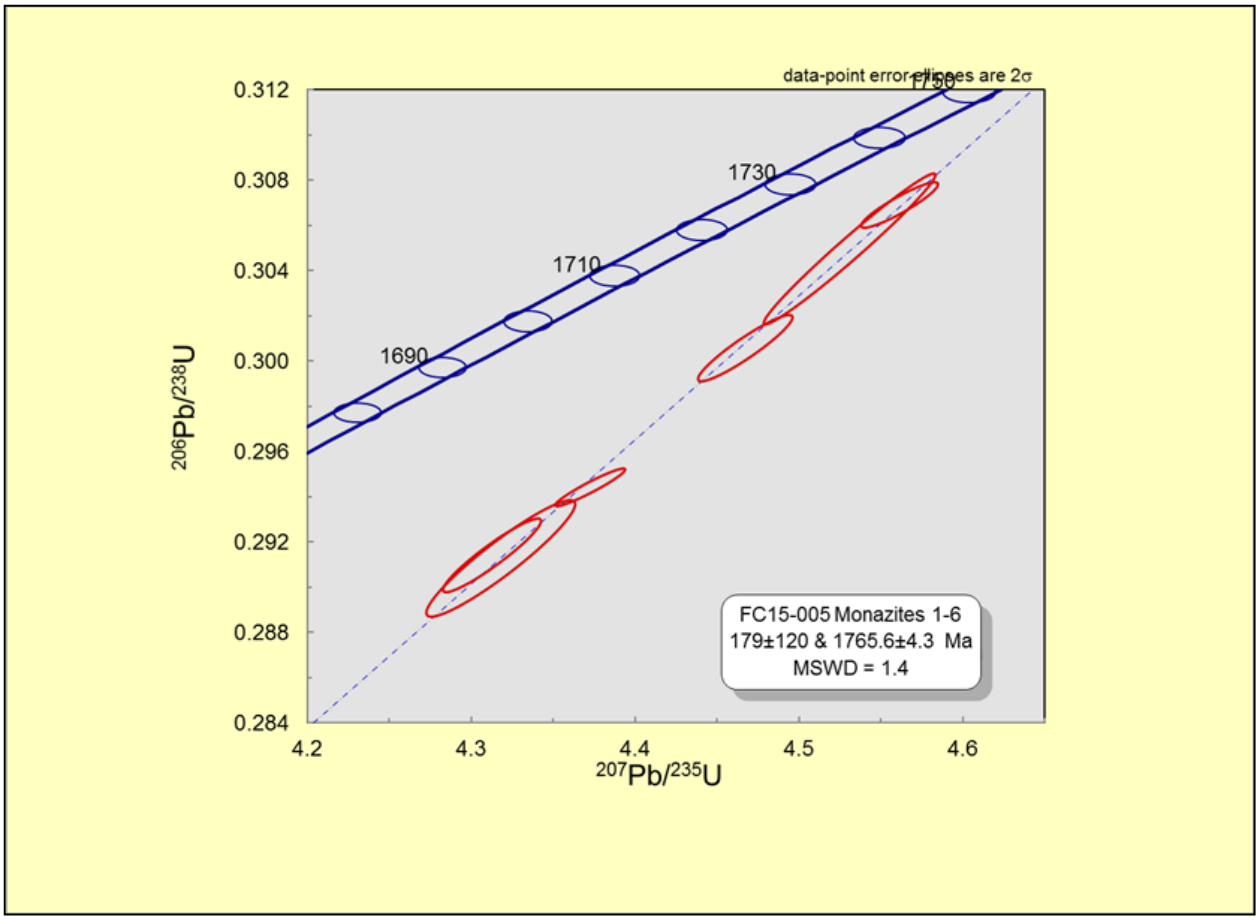

Figure B5. Concordia Diagram for FC15-005 monazites.

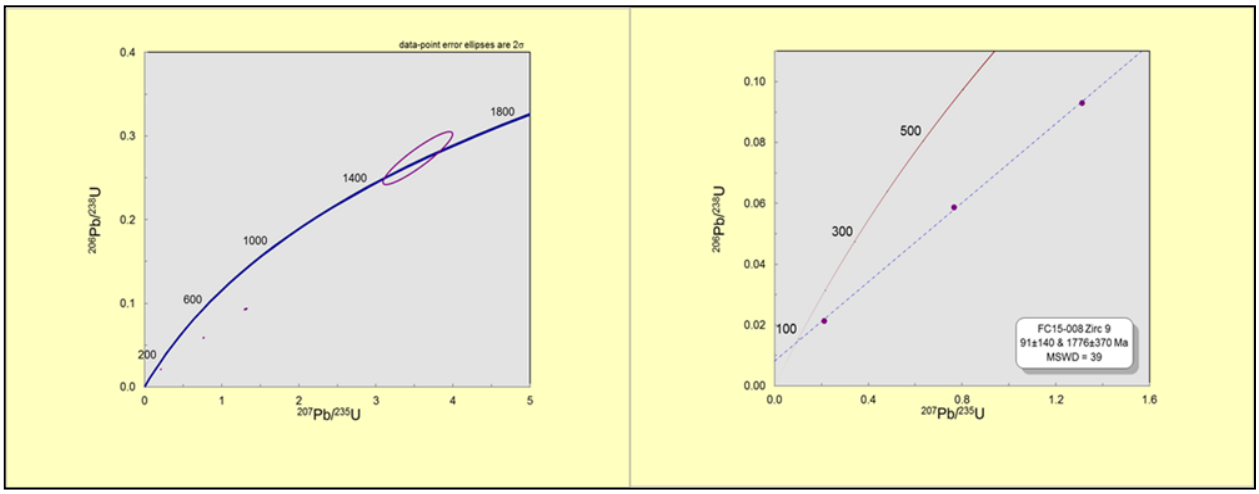

Figure B6. Concordia diagrams for FC15-008 zircon 9. The large error ellipse above concordia show on the left diagram represents the HCl wash. The dates of 1776±370 and 91±140 Ma, shown on right, exclude the HCl wash analyses. The error ellipses are smaller than the circles representing them on the right diagram.

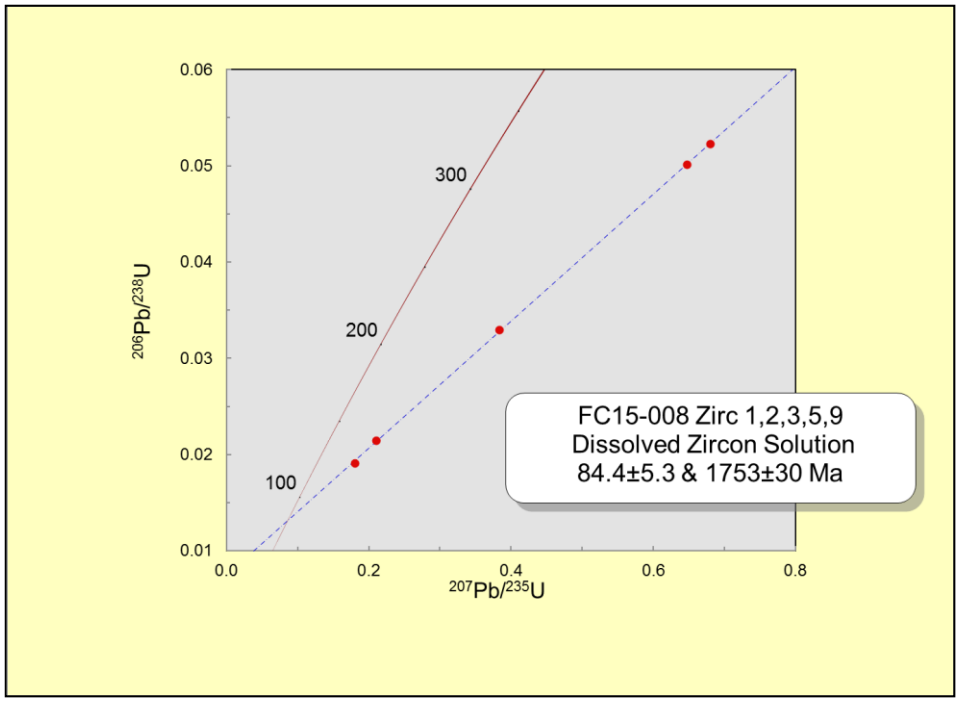

Figure B7. Concordia diagram for FC15-008 zircons. The final dissolved zircon solution (step 4) analyses were plotted to constrain dates of 1753±30 and 84.4±5.3 Ma. Error ellipses are smaller than the circles representing them.

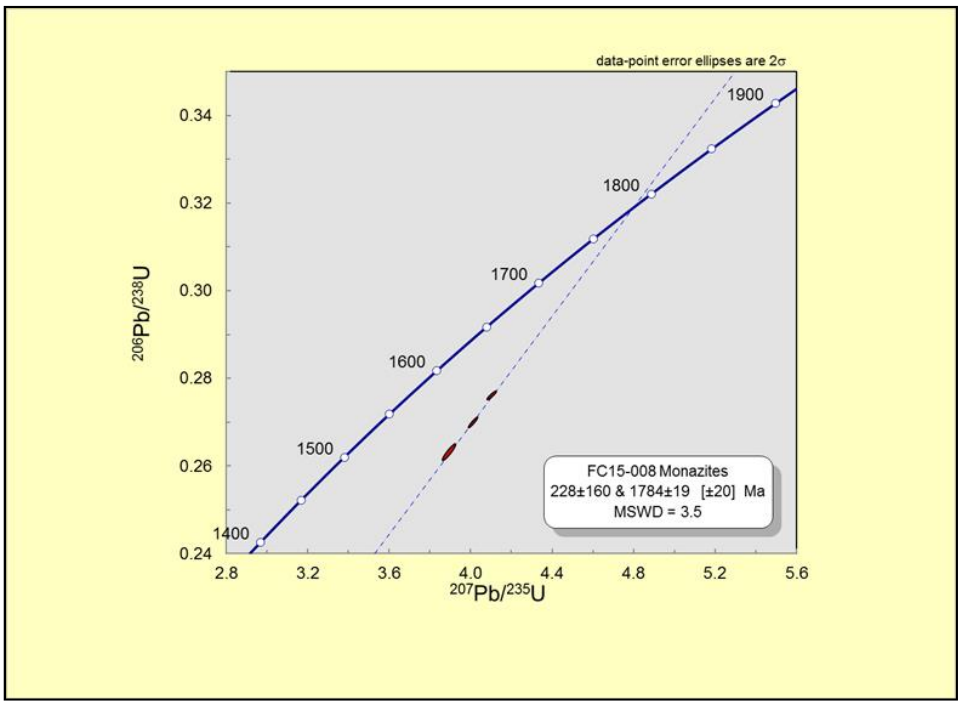

Figure B8. FC15-008 Concordia diagram for FC15-008 monazites.

Table 2. Results of U-Pb dating for two Highland Mountains granatoid dikes.

		Compositional Parameters								Radiogenic Isotope Ratios							
Sample	Wt. mg	U ppm	Th/U	Pb ppm	^{206}Pb* mol % |0^{-13} m ^{206}Pb*	Pb*/Pbc	Pbc (pg)	^{206}Pb/^{204}Pb	^{208}Pb/^{206}Pb	^{207}Pb/^{206}Pb	% err	^{207}Pb/^{235}U	% err	^{206}Pb/^{238}U	% err	corr. coef.
(a)	(b)	(c)	(d)	(c)	(e)	(e)	(e)	(f)	(g)	(g)	(h)	(g)	(h)	(g)	(h)	
(Z35) FC15-005 HF+HNO3 Leach	0	1134.68	0.422	239.486	6.35	0.881	2.337	71.8	150.338	0.176	0.104	0.99	1.929	1.236	0.134	0.457	0.67
(Z1) FC15-005 Zirc 1 Chemical Abrasion	0	79723.4	0.17	4179.98	157	0.975	11.18	343	703.7	0.089	0.095	0.346	0.617	1.043	0.047	0.927	0.945
(Z12) FC15-005 Zirc 1 HCl Wash	0	5.63928	0.386	6.04341	0.1	0.707	0.697	3.56	61.5093	0.083	0.082	7.394	4.969	29.83	0.439	28.77	0.969
(Z59) FC15-005 Zirc 1 Dissolved Zircon	0	15199.6	0.228	3937.31	161	0.999	308.7	12.7	18990.8	0.074	0.107	0.184	3.763	1.089	0.254	1.042	0.986
(Z36) FC15-005 Zirc 2 HF+HNO3 Leach	0	1542.43	1.721	595.361	9.91	0.786	1.647	225	83.8138	0.699	0.109	1.429	2.317	1.634	0.154	0.525	0.527
(Z11) FC15-005 Zirc 2 Chemical Abrasion	0	59471.6	0.319	5073.76	184	0.982	16.85	284	983.803	0.161	0.104	0.251	1.063	3.278	0.074	3.254	0.997
(Z13) FC15-005 Zirc 2 HCl Wash	0	3.43593	1.792	16.1256	0.2	0.61	0.511	10.7	46.0652	0.213	0.104	4.108	20.06	39.39	1.399	39.15	0.995
(Z60) FC15-005 Zirc 2 Dissolved Zircon	0	19333.7	0.268	5152.51	207	0.999	222.9	23	13465.3	0.089	0.114	0.184	4.025	0.533	0.256	0.43	0.95
(Z39) FC15-005 Zirc 3 HF+HNO3 Leach	0	62.4902	0.272	14.2728	0.18	0.625	0.549	9.21	47.8602	0.18	0.151	3.583	1.474	4.675	0.071	2.833	0.643
(Z30) FC15-005 Zirc 3 Chemical Abrasion	0	1072.43	0.153	245.181	9.56	0.988	23.5	10	1448.11	0.06	0.133	0.258	3.913	0.971	0.214	0.894	0.965
(Z14) FC15-005 Zirc 3 HCl Wash	0	0.32838	1.786	1.94183	0.03	0.686	0.704	1.14	58.109	0.164	0.122	28.19	37.23	36.55	2.208	23.04	0.636
(Z61) FC15-005 Zirc 3 Dissolved Zircon	0	7341.08	0.246	2741.65	108	0.999	606.5	4.51	35941.6	0.078	0.148	0.16	7.211	0.44	0.354	0.318	0.962
(Z45) FC15-005 Zirc 4 HF+HNO3 Leach	0	30.6669	0.453	34.7388	0.85	0.849	1.753	12.6	118.972	0.101	0.158	0.795	14.52	1.047	0.666	0.497	0.684
(Z31) FC15-005 Zirc 4 Chemical Abrasion	0	587.175	0.386	355.494	9.05	0.86	1.891	123	128.086	0.114	0.132	1.22	6.704	2.04	0.37	1.635	0.801
(Z15) FC15-005 Zirc 4 HCl Wash	0	0.78844	2.481	9.28486	0.11	0.606	0.496	6.21	45.6134	0.168	0.134	4.405	64.51	70.98	3.484	70.83	0.998
(Z62) FC15-005 Zirc 4 Dissolved Zircon	0	4740.12	0.362	1891.89	72.2	0.998	191.7	9.82	11031.8	0.113	0.15	0.202	7.537	0.444	0.365	0.304	0.921
(Z46) FC15-005 Zirc 5 HF+HNO3 Leach	0	44.7576	0.694	23.2902	0.38	0.718	0.876	12.4	63.6224	0.268	0.123	2.269	3.436	2.578	0.203	0.75	0.533
(Z32) FC15-005 Zirc 5 Chemical Abrasion	0	2447.64	0.089	382.774	15.4	0.988	24.65	14.9	1559.27	0.039	0.122	0.226	2.533	1.14	0.151	1.081	0.981
(Z16) FC15-005 Zirc 5 HCl Wash	0	0.53171	-0.15	1.69543	0.01	0.449	0.22	1.39	32.9712	-0.03	0.113	185.5	9.645	200.5	0.618	75.54	0.38
(Z63) FC15-005 Zirc 5 Dissolved Zircon	0	5280.44	0.158	1619.6	65.5	0.999	412	3.92	25031.9	0.054	0.142	0.183	5.83	0.43	0.297	0.294	0.941
(Z48) FC15-005 Zirc 7 HF+HNO3 Leach	0	40.1135	0.422	14.4708	0.3	0.785	1.141	6.76	83.4947	0.159	0.105	1.642	2.567	2.784	0.177	2.125	0.809
(Z37) FC15-005 Zirc 7 Chemical Abrasion	0	962.766	0.305	264.08	8.85	0.945	5.158	42.9	326.717	0.105	0.107	0.448	3.245	0.878	0.22	0.645	0.87
(Z18) FC15-005 Zirc 7 HCl Wash	0	0.2369	5.972	13.0866	0.02	0.109	0.048	12.5	20.1455	0.508	0.067	119.7	17.24	390.6	1.859	371.5	0.952
(Z67) FC15-005 Zirc 7 Dissolved Zircon	0	2066.55	0.269	533.701	21.1	0.993	39.96	13	2443.98	0.088	0.107	0.213	3.619	0.556	0.245	0.433	0.937
(Z50) FC15-005 Zirc 9 HF+HNO3 Leach	0	115.814	0.476	44.7711	0.92	0.79	1.201	20.3	85.5914	0.177	0.11	1.643	2.884	1.91	0.19	0.624	0.56
(Z40) FC15-005 Zirc 9 Chemical Abrasion	0	2887.9	0.305	576.836	21.2	0.976	12.29	43.4	748.4	0.115	0.105	0.297	2.558	1.917	0.176	1.867	0.988
(Z20) FC15-005 Zirc 9 HCl Wash	0	5.78915	0.777	16.0328	0.12	0.443	0.254	12.8	32.2254	0.178	0.11	7.752	7.692	28.35	0.505	27.22	0.962
(Z69) FC15-005 Zirc 9 Dissolved Zircon	0	4931.05	0.311	1320.77	52.1	0.995	54.85	23.7	3313.12	0.101	0.107	0.185	3.738	0.752	0.253	0.676	0.972 1758
(Z51) FC15-008 Zirc 1 HF+HNO3 Leach	0	1044.68	1.187	127.615	0.2	0.121	0.066	120	20.3727	0.827	0.103	38.31	0.064	39.71	0.005	12.15	0.266
(Z41)FC15-008 Zirc 1 Chemical Abrasion	0	46141.8	0.168	982.991	28.7	0.884	2.11	316	153.81	0.067	0.06	1.285	0.124	2.767	0.015	2.357	0.886
(Z21) FC15-008 Zirc 1 HCl Wash	0	14.7659	0.681	10.183	0.12	0.573	0.413	7.21	42.0476	0.181	0.063	10.59	1.624	11.56	0.188	3.448	0.417
(Z70) FC15-008 Zirc 1 Dissolved Zircon	0	14284	0.074	264.401	11.4	0.994	44.68	5.79	2966.42	0.033	0.068	0.257	0.18	1.914	0.019	1.876	0.991
(Z52) FC15-008 Zirc 2 HF+HNO3 Leach	0	493.208	1.057	373.003	0.28	0.061	0.035	360	19.0796	1.035	0.159	52.41	0.299	53.11	0.014	26.6	0.277
(Z42) FC15-008 Zirc 2 Chemical Abrasion	0	165072	0.051	4808.07	180	0.955	5.827	704	399.918	0.026	0.082	0.941	0.294	2.528	0.026	2.33	0.928
(Z22) FC15-008 Zirc 2 HCl Wash	0	570.122	0.093	59.9818	1.35	0.796	1.073	28.9	87.784	0.039	0.076	2.209	0.596	2.473	0.057	0.671	0.508
(Z71) FC15-008 Zirc 2 Dissolved Zircon	0	33293.7	0.031	1695.97	72.6	0.994	47.3	35.1	3111.12	0.016	0.094	0.23	0.68	0.585	0.052	0.465	0.929
(Z53) FC15-008 Zirc 3 HF+HNO3 Leach	0	3419.77	1.778	268.211	1.13	0.293	0.18	227	25.3566	0.693	0.057	31.62	0.063	34.25	0.008	6.529	0.483
(Z43) FC15-008 Zirc 3 Chemical Abrasion	0	164287	0.095	4133.35	152	0.952	5.532	633	376.846	0.044	0.074	0.578	0.227	8.509	0.022	8.479	0.998
(Z23) FC15-008 Zirc 3 HCl Wash	0	196.917	0.218	55.8217	1.82	0.915	2.967	14.1	211.631	0.053	0.059	1.035	1.813	1.47	0.222	0.852	0.725
(Z72) FC15-008 Zirc 3 Dissolved Zircon	0	20930.7	0.026	658.094	28.8	0.997	84.71	7.68	5624.21	0.013	0.084	0.222	0.383	0.596	0.033	0.487	0.936
(Z56) FC15-008 Zirc 5 HF+HNO3 Leach	0	1720.22	1.791	653.749	0.21	0.027	0.021	641	18.4045	1.881	0.156	131.5	0.062	133.9	0.003	61.01	0.267
(Z54)FC15-008 Zirc 5 Chemical Abrasion	0	101474	0.087	2195.46	62.6	0.871	1.831	776	138.783	0.036	0.064	1.345	0.13	3.207	0.015	2.829	0.908
(Z25) FC15-008 Zirc 5 HCl Wash	0	17.7514	0.34	18.232	0.17	0.493	0.273	14.3	35.4129	0.078	0.055	13.85	1.725	14.62	0.226	2.581	0.378
(Z74) FC15-008 Zirc 5 Dissolved Zircon	0	2447.44	0.026	119.225	5.12	0.994	48.56	2.41	3208.18	0.013	0.094	0.196	0.648	0.455	0.05	0.304	0.944
(Z66) FC15-008 Zirc 9 HF+HNO3 Leach	0	705.578	0.09	87.1382	2.74	0.91	2.863	22.6	199.593	0.042	0.102	0.72	1.311	1.032	0.093	0.568	0.742
(Z63)FC15-008 Zirc 9 Chemical Abrasion	0	29127.1	0.051	1743.68	71.3	0.984	16.72	98.4	1101.63	0.025	0.095	0.355	0.766	0.663	0.059	0.475	0.856
(Z29) FC15-008 Zirc 9 HCl Wash	0	11.9994	0.228	8.78002	0.14	0.674	0.595	5.51	55.2176	0.066	0.094	4.255	3.544	10.39	0.274	9.368	0.912
(Z79) FC15-008 Zirc 9 Dissolved Zircon	0	6208.69	0.076	129.78	5.55	0.993	38.14	3.32	2525.62	0.034	0.071	0.282	0.211	0.468	0.021	0.245	0.87
(BB) FC15-005 Mnz 1	0	6569.4	21.71	12941.1	79.8	0.97	61.39	207	593.852	6.571	0.108	0.318	4.318	0.86	0.291	0.726	0.933
(BC) FC15-005 Mnz 2	0	7880.89	28.26	19764.6	100	0.998	1509	13.1	11488.1	8.372	0.108	0.186	4.531	0.947	0.305	0.892	0.981
(BI) FC15-005 Mnz 3	0	14209.6	31.86	38883.5	175	0.998	1163	33.4	7835.57	9.602	0.108	0.191	4.373	0.398	0.294	0.233	0.95
(BJ) FC15-005 Mnz 4	0	22145.2	32.97	63337.1	278	0.993	383	165	2537.86	9.837	0.108	0.215	4.467	0.528	0.301	0.397	0.93
(BM) FC15-005 Mnz 5	0	10117.3	30.79	26685.5	123	0.994	459.1	58	3192.19	9.308	0.107	0.215	4.313	0.571	0.291	0.456	0.937
(BO) FC15-005 Mnz 6	0	11477.4	23.62	24701.1	147	0.998	1202	20.5	10725.5	6.977	0.108	0.21	4.561	0.424	0.307	0.265	0.914
(BP) FC15-008 Mnz 1	0	16764.3	26.39	36414.3	184	0.994	386.3	94	2948.97	8.384	0.107	0.266	3.898	0.7	0.263	0.592	0.929
(ZR1) FC15-008 Mnz 4	0	2304.12	28.6	5457.5	26	0.997	769.9	7.08	5508.01	8.997	0.108	0.189	4.015	0.483	0.27	0.358	0.942
(ZR3) FC15-008 Mnz 5	0	3152.79	25.49	6682.47	34.8	0.993	305.1	21.8	2402.75	8.108	0.108	0.211	3.938	4.536	0.264	4.523	0.999
(ZR14) FC15-008 Mnz 7	0	5181.94	24.6	10879.1	59.7	0.998	1408	7.72	11598.2	7.655	0.108	0.201	4.108	0.438	0.276	0.293	0.924

(a) z1, z2 etc. are labels for fractions composed of single zircon grains or fragments; all fractions annealed and chemically abraded after Mattinson (2005).
(b) Nominal fraction weights estimated from photomicrographic grain dimensions, adjusted for partial dissolution during chemical abrasion.
(c) Nominal U and total Pb concentrations subject to uncertainty in photomicrographic estimation of weight and partial dissolution during chemical abrasion.
(d) Model Th/U ratio calculated from radiogenic 208Pb/206Pb ratio and 207Pb/235U age.
(e) Pb* and Pbc represent radiogenic and common Pb, respectively; mol % ^{206}Pb* with respect to radiogenic, blank and initial common Pb.
(f) Measured ratio corrected for spike and fractionation only.
(g) Corrected for fractionation, spike, and common Pb; up to 1 pg of common Pb was assumed to be procedural blank: 206Pb/204Pb = 18.60 ± 0.80%; 207Pb/204Pb = 15.69 ± 0.32%
(h) Errors are 2-sigma, propagated using the algorithms of Schmitz and Schoene (2007) and Crowley et al. (2007).
(i) Calculations are based on the decay constants of Jaffey et al. (1971). 206Pb/238U and 207Pb/206Pb ages corrected for initial disequilibrium in 230Th/238U using Th/U [magma] =
(j) Corrected for fractionation, spike, and blank Pb only.

Daly analyses, based on analysis of NBS-981 and NBS-982.
208Pb/204Pb = 38.51 ± 0.74% (all uncertainties 1-sigma). Excess over blank was assigned to initial common Pb.

Appendix C

GRAIN IMAGING

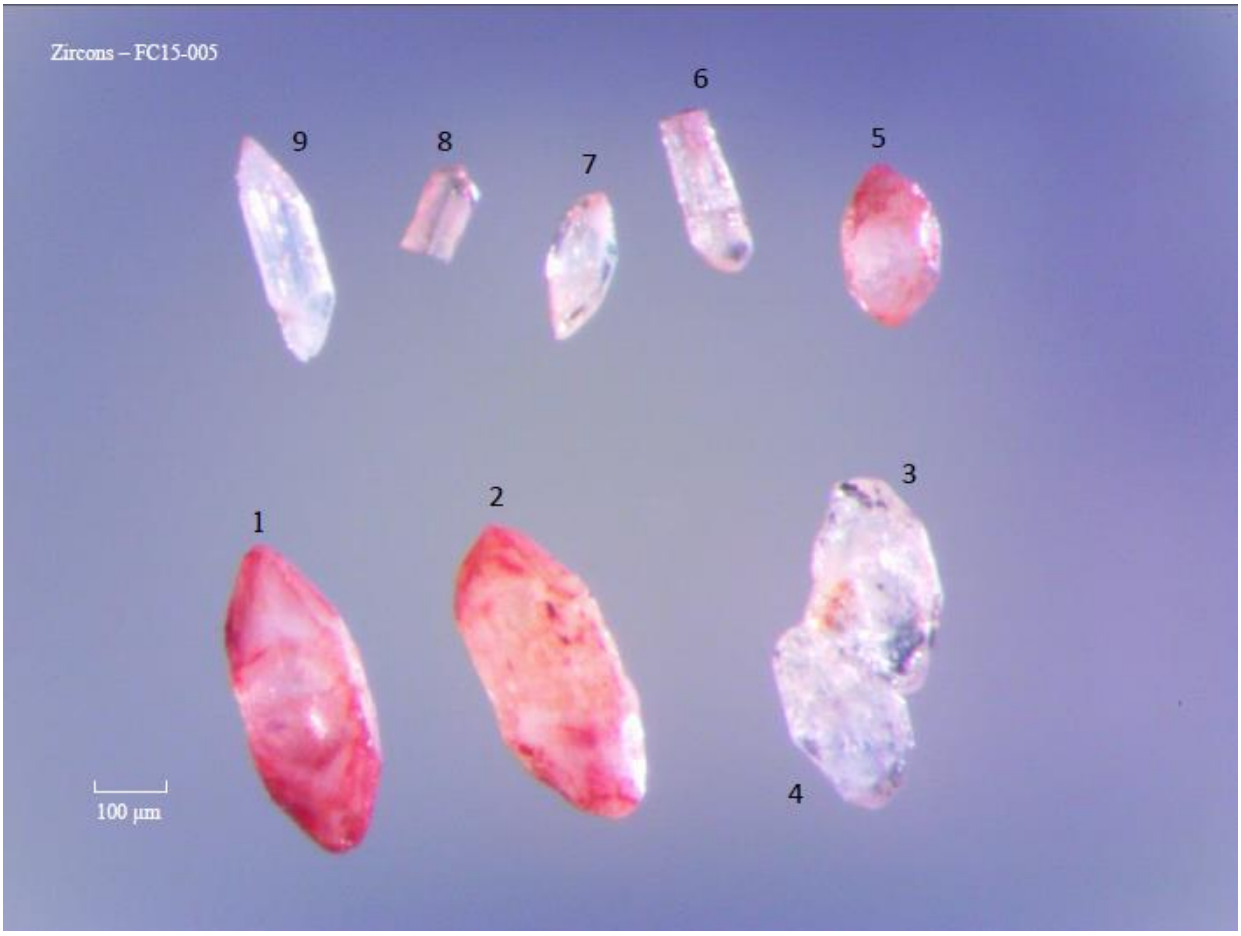

Figure C1. Image of zircons from FC15-005 used for TIMS analysis. Red discoloring suggests Pb loss from radiation damage.

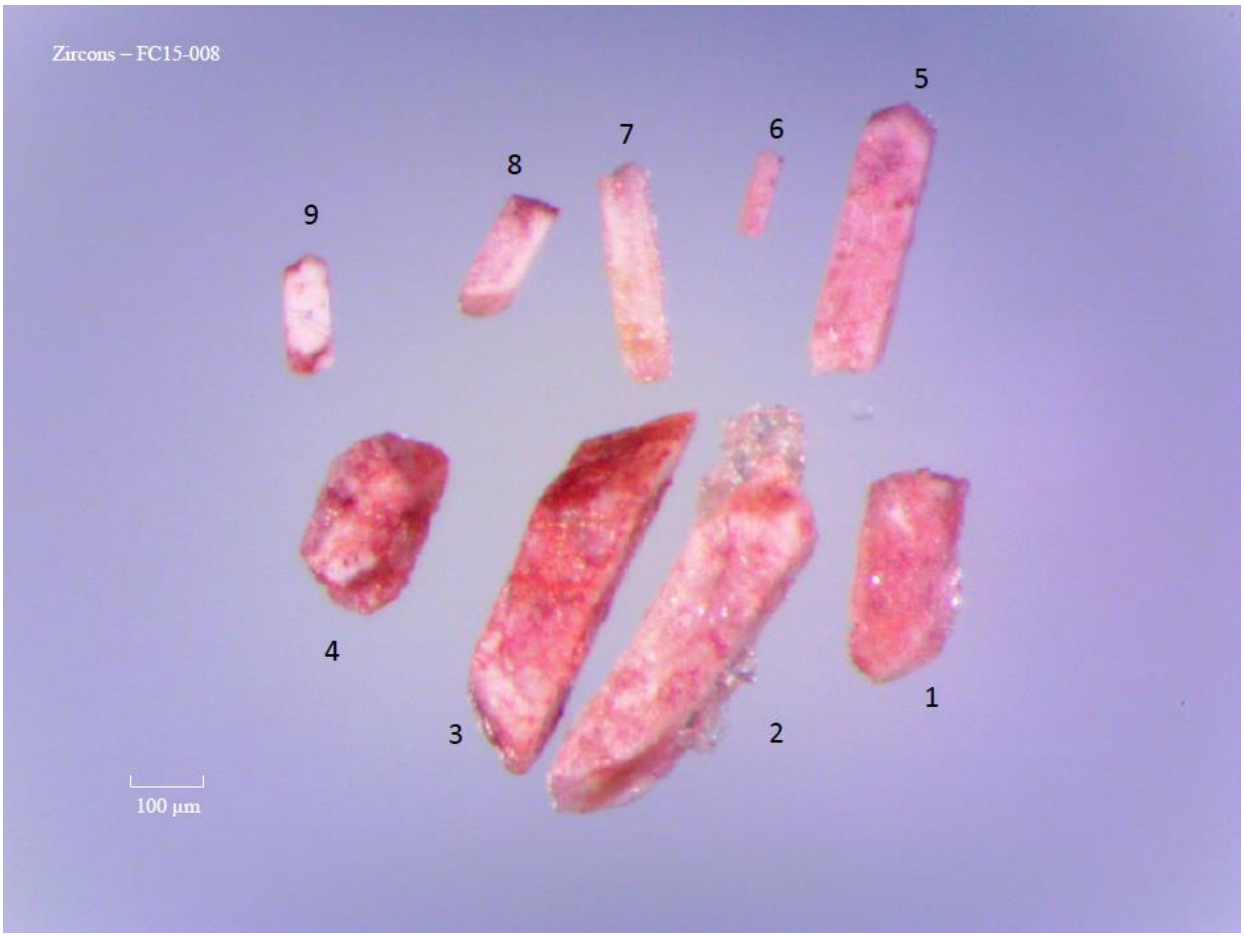

Figure C2. Image of zircons from FC15-008 used in TIMS analysis. All grains show extreme damage and red discoloration which suggests major Pb-loss.

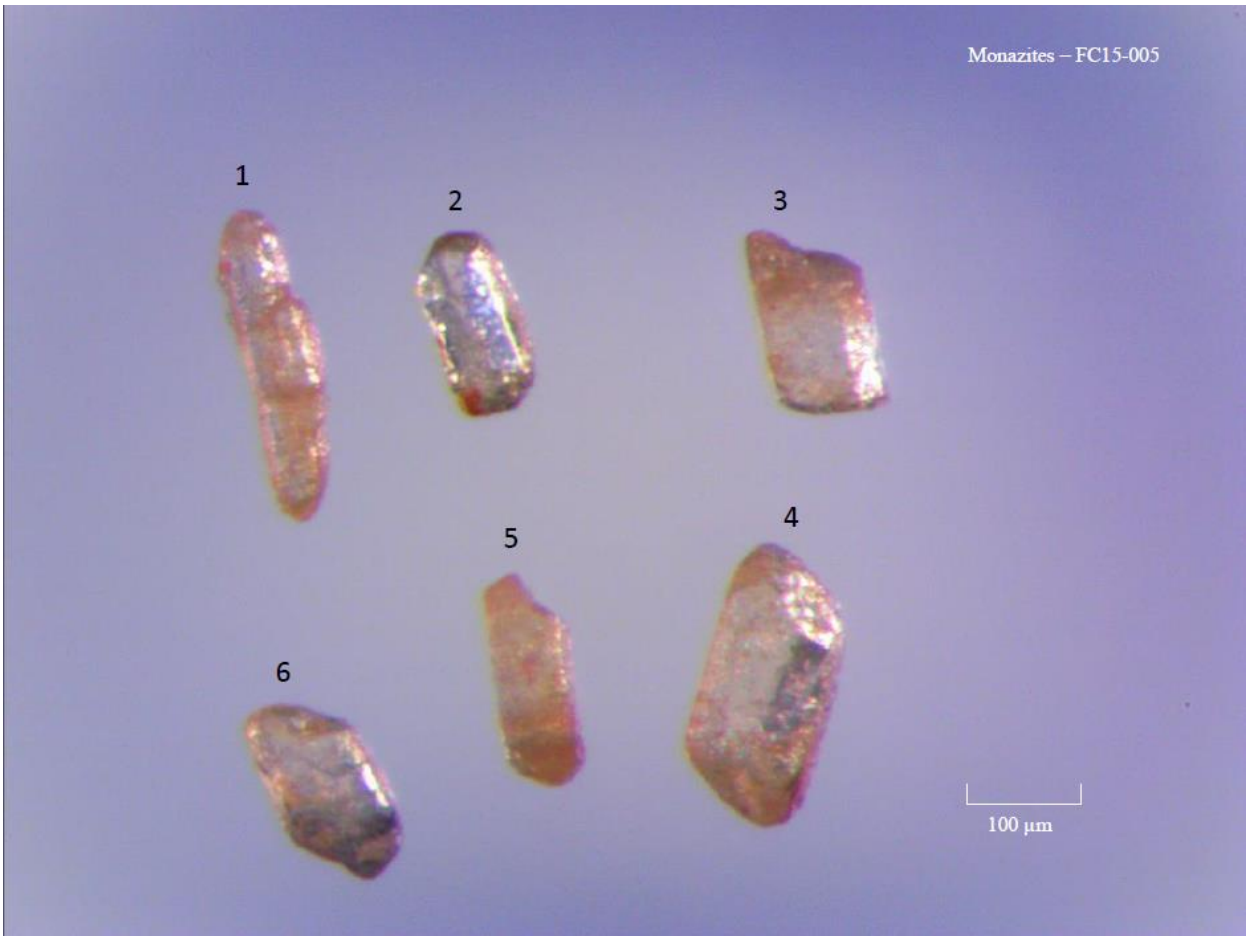

Figure C3. Image of monazite grains from FC15-005 used in TIMS analysis.

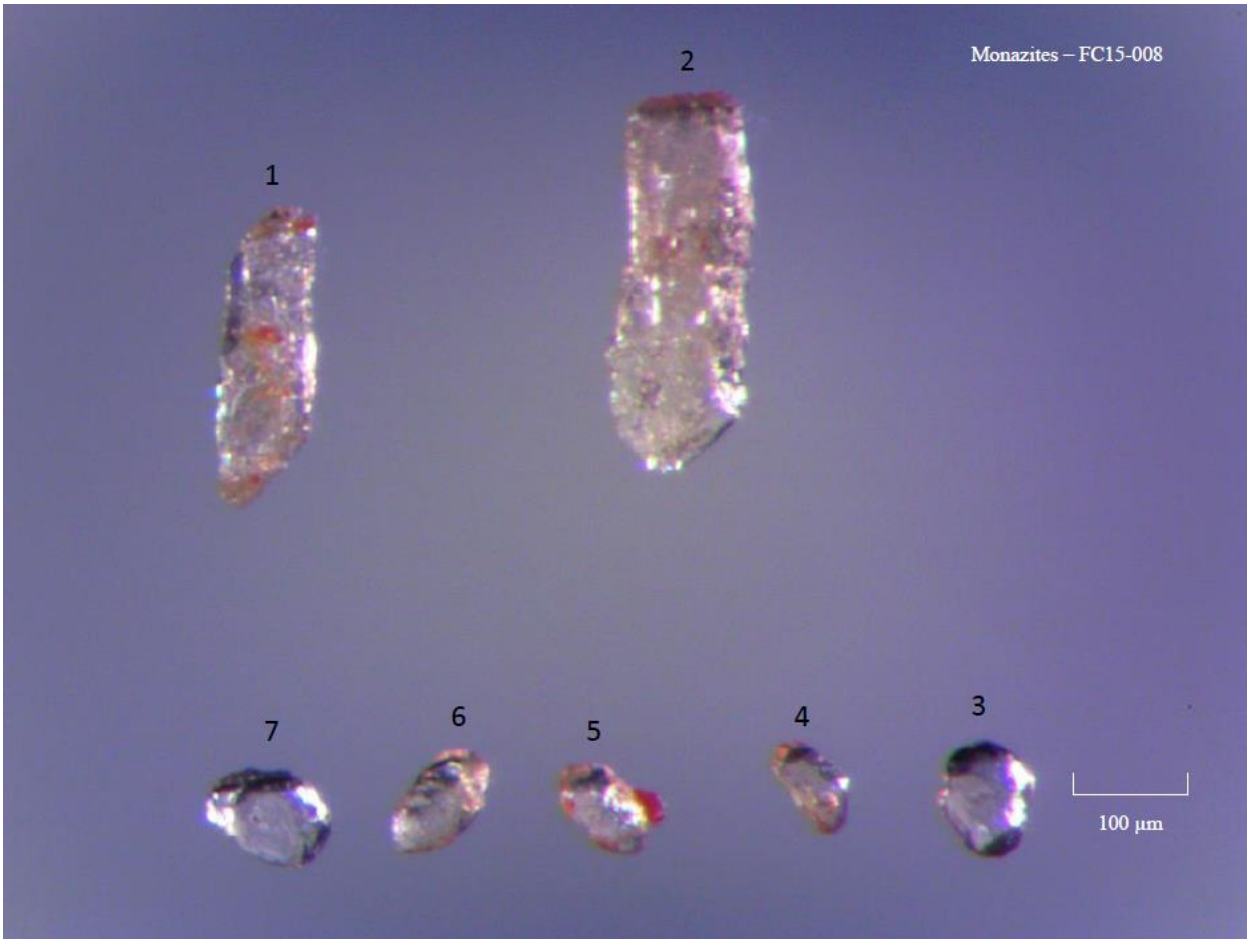

Figure C4. Image of monazite grains from FC15-008 used in TIMS analysis. Two distinct variations of monazites are present, however, analysis showed no differences in age (see fig. B20).

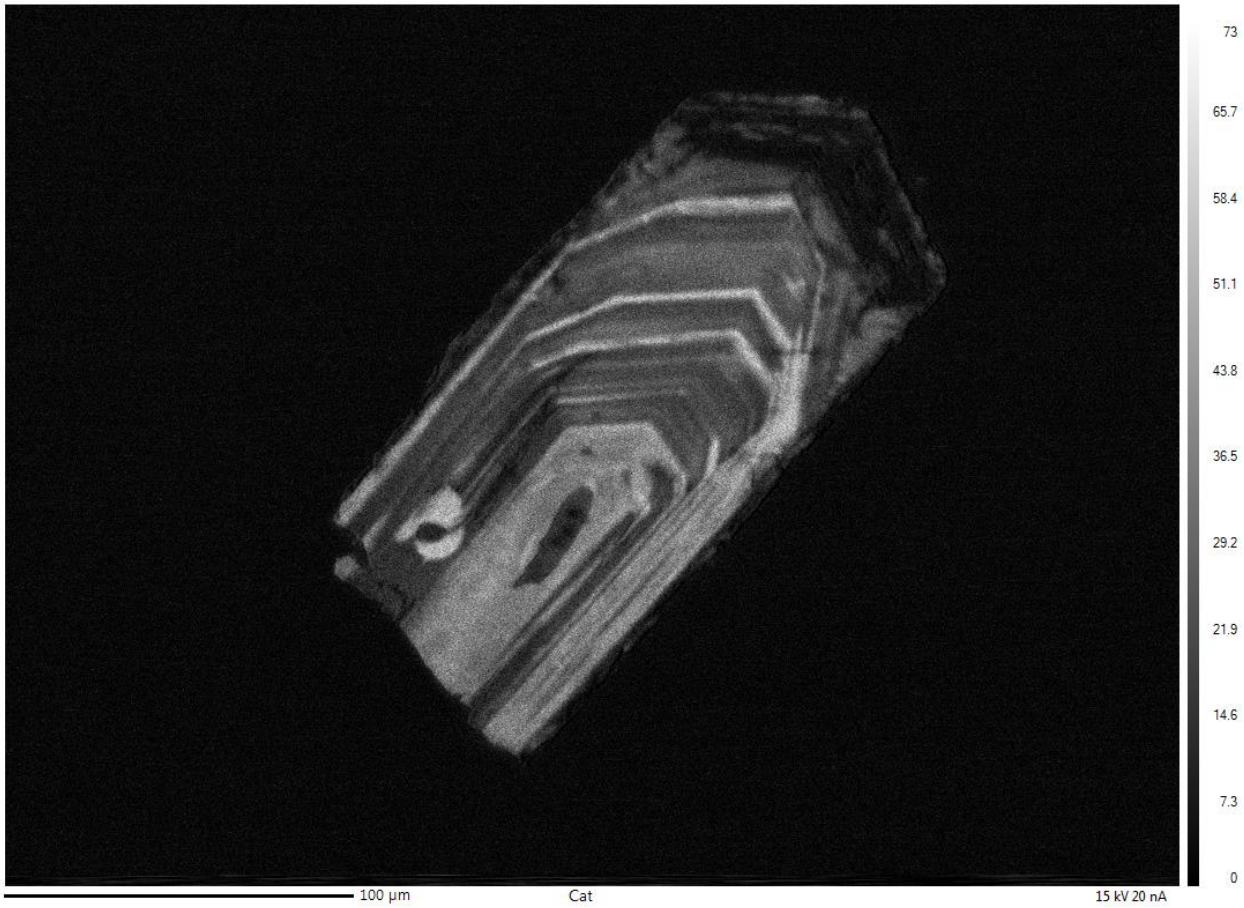

Figure C5. CL image of a zircon grain from FC15-005 shows a zoning pattern that is consistent throughout the grain which suggests the core and subsequent rims crystallized during the same time. The inclusion in the center of the core is apatite which was analyzed by EDS.

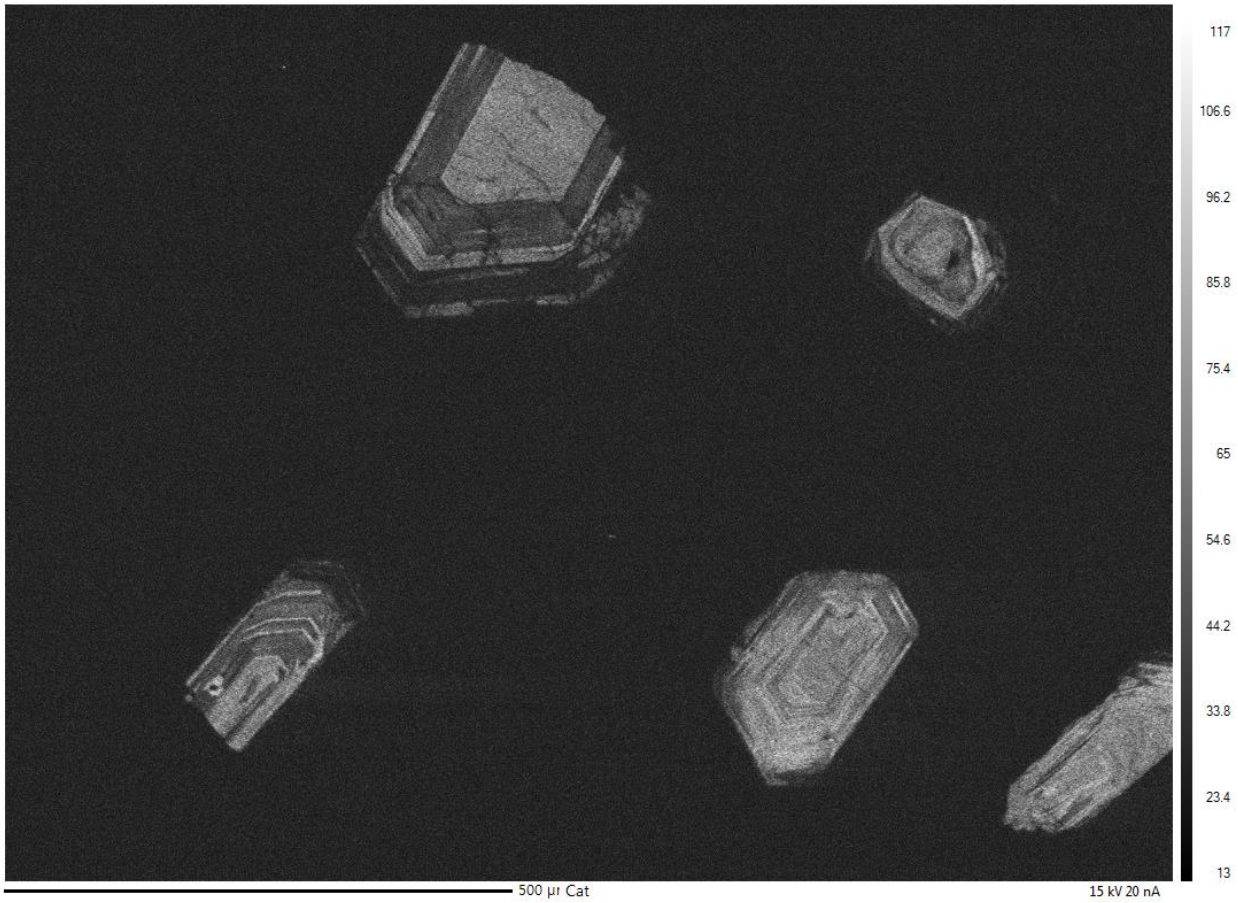

Figure C6. CL image of multiple zircon grains from FC15-005 showing core to rim zoning patterns.

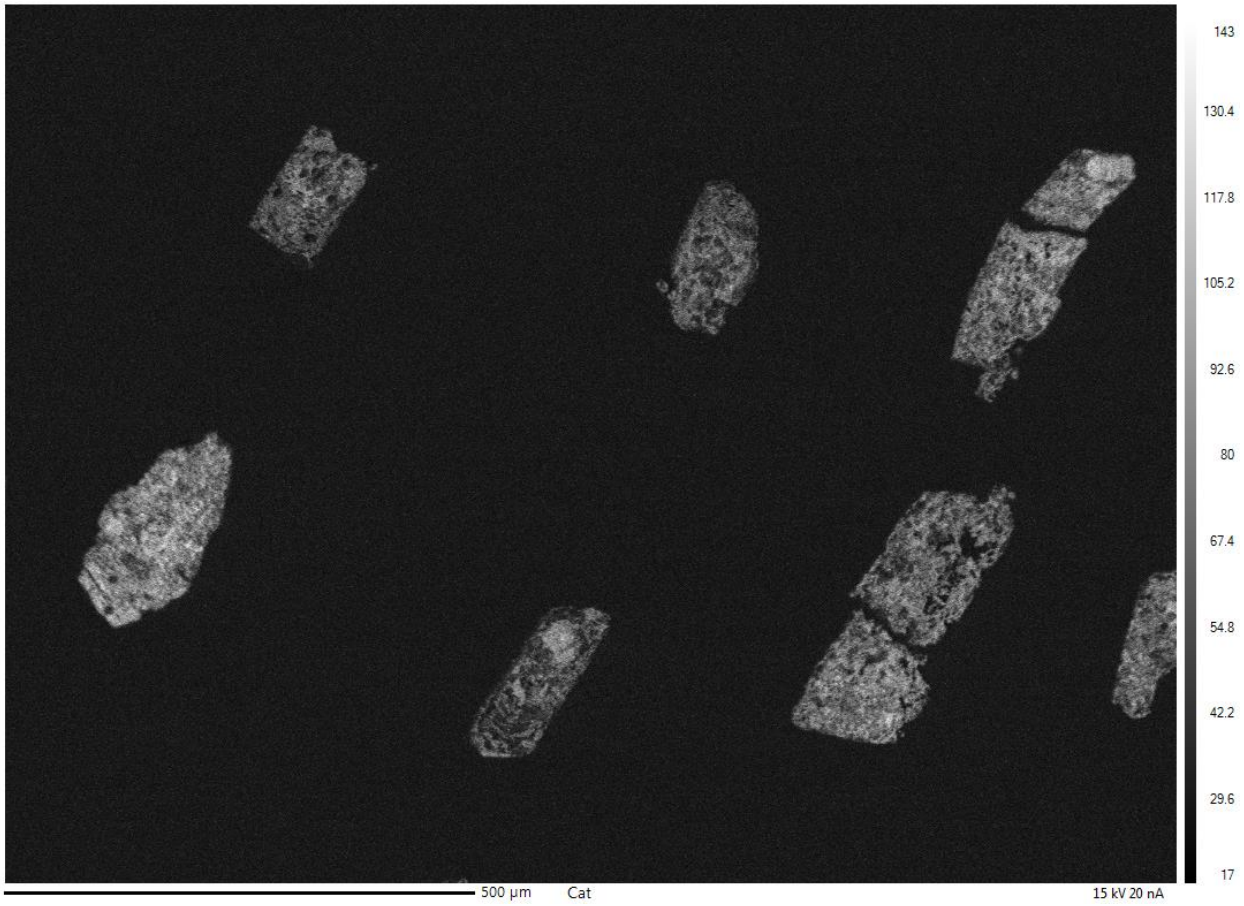

Figure C7. CL images of zircons from FC15-008. No internal structure or core-rim zoning is present.

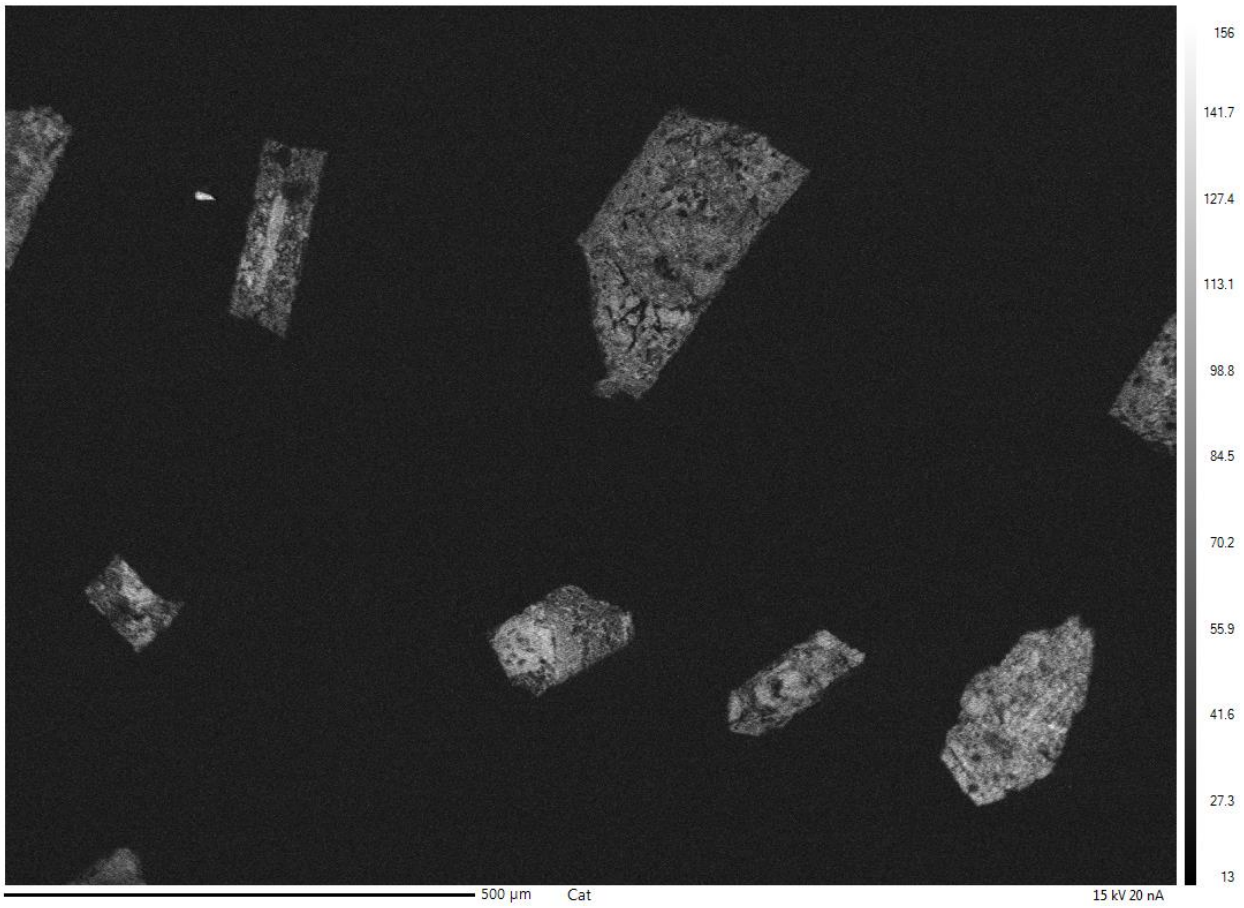

Figure C8. CL images of zircons from FC15-008. Internal damage extends to all grains observed. Zoning patterns cannot be confidently found in any zircons.

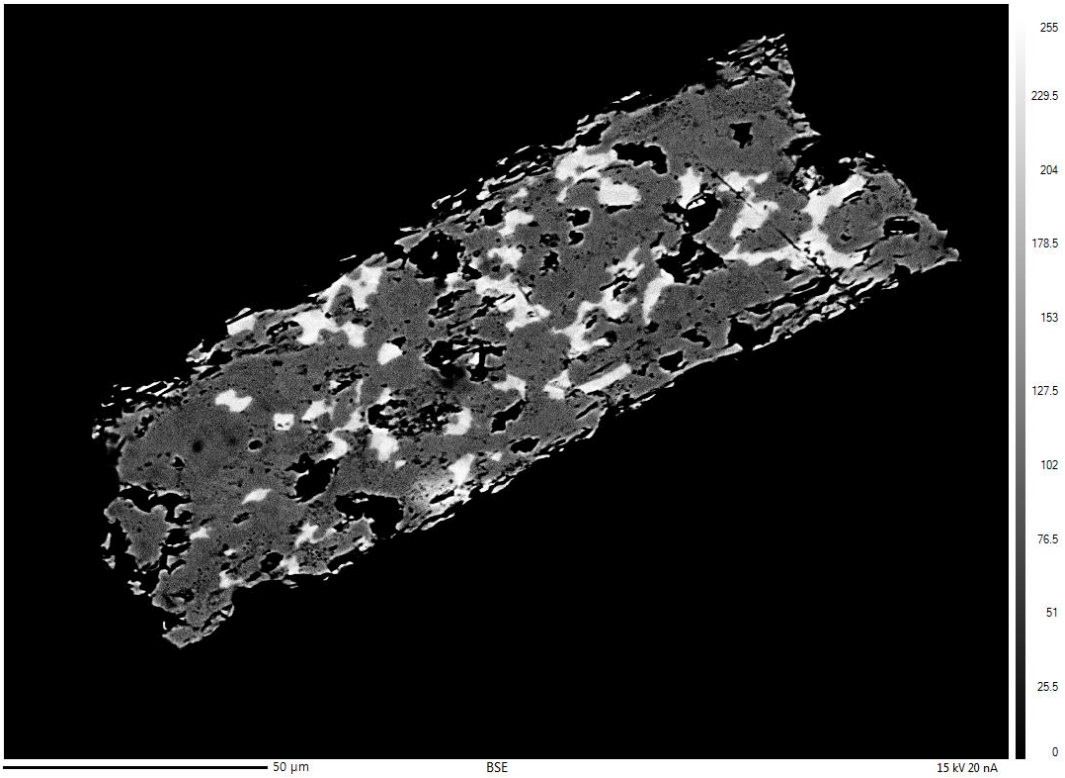

Figure C9. Back-scatter image of a monazite grain from FC15-008. The light colored inclusions are the mineral xenotime and were analyzed with EDS.